



UNIVERSIDADE D
COIMBRA

Miguel Alexandre Gomes Duarte

**COMPUTATIONAL MODELLING
FOR BONE TISSUE ENGINEERING**

A FLUID DYNAMICS ANALYSIS FOR ILIAC BONE SCAFFOLDS

**Thesis submitted to the Faculty of Science and Technology of the University
of Coimbra for the degree of Master in Biomedical Engineering with
specialization in Biomedical Instrumentation, supervised by Prof. Dr. Paula
Pascoal-Faria and Prof. Dr. Miguel Morgado**

Maio de 2023

• U



C •

FCTUC

FACULDADE DE CIÊNCIAS
E TECNOLOGIA

UNIVERSIDADE DE COIMBRA

Miguel Duarte

**Computational Modelling for Bone Tissue Engineering:
A Fluid Dynamics Analysis for Iliac Bone Scaffolds**

Thesis submitted to the
University of Coimbra for the degree of
Master in Biomedical Engineering

Supervisors:
Prof. Dr. Miguel Morgado
Prof^ª. Dr^ª. Paula Pascoal-Faria

Coimbra, 2023

This work was developed in collaboration with:



This thesis is part of the FCT Project *OptioBioScaffold*:
(PTDC/EME-SIS/4446/2020), leaded by Professor Paula Pascoal-Faria

Effect of geometrical features in biodegradable scaffolds for tissue tissue engineering: a numerical analysis, 8th edition of the Symposium on Computational Tools for Direct Digital Manufacturing (CT4DDM), held within the 21st International Conference of Numerical Analysis and Applied Mathematics (ICNAAM) – oral communication, Crete, Greece, 19-25th september, 2022

Effect of geometrical features in biodegradable scaffolds for tissue tissue engineering: a numerical analysis, Conf. Proceedings, American Institute of Physics (accepted for publication), 2022

Studying the impact of the geometry of bioscaffolds in the wall shear stress distribution for iliac bone regeneration - oral presentation at the joint international symposium of the research work developed at the university of Shannon, Ireland and at the CDRSP, Polytechnic of Leiria, Athlone, Ireland, 18th july 2023

Esta cópia da tese é fornecida na condição de que quem a consulta reconhece que os direitos de autor são pertença do autor da tese e que nenhuma citação ou informação obtida a partir dela pode ser publicada sem a referência apropriada.

This copy of the thesis has been supplied on condition that anyone who consults it is understood to recognize that its copyright rests with its author and that no quotation from the thesis and no information derived from it may be published without proper acknowledgement.

Agradecimentos

Quero agradecer à professora Paula Pascoal-Faria, por toda a supervisão ao longo deste projeto, e ao professor Miguel Morgado, pela disponibilidade em criar pontes de colaboração entre a Faculdade de Ciências e Tecnologia da Universidade de Coimbra e o Centro de Desenvolvimento Rápido e Sustentado de Produto do Politécnico de Leiria, permitindo a oportunidade única de integrar o promissor campo de investigação da Engenharia de Tecidos. Ao João Meneses, quero agradecer o apoio e conhecimento no uso das ferramentas de simulação, em fases críticas da elaboração desta dissertação.

Ao João Ajuda e ao Diogo Loureiro Martinho, amigos dedicados, obrigado pela prontidão e espírito crítico com que me aconselharam ao longo deste projeto.

Por fim, obrigado à minha família.

Abstract

Bone Tissue Engineering (BTE) has emerged as a clinical research field focused on bone tissue defects regeneration using porous biodegradable scaffolds that provide mechanical support, offering the adhesion sites for the bone cells to proliferate. One aim of Tissue Engineering (TE) is the culture of living cells within devices and scaffolds that create a mimicked bone tissue growth environment. In that regard, some key aspects have been identified as of major relevance: the interactions of cells with the surrounding extra-cellular membrane (ECM) and other cells, in which ECM modulates cell proliferation, differentiation, and metabolic functions; and the influence of environmental factors such as mechanical (e.g., flow-induced effects), electrical and biochemical stimuli. A gap between architecture and biological response of these bone graft substitutes exists because each construct must fulfill specific resorption and biodegradation rates, bone in-growth and mechanical support parameters, as well as applying the material composition and solubility to patients and implantation sites. A dense scaffold aims for a increased mechanical role, while a highly porous enhance cell delivery, or a permeable construct favors transport of nutrients and waste products. The optimum scaffold architecture appears as a relative concept, since different settings increase different functions and diminish others.

As a complement to the *in vitro* research on the influence of these aspects, the use of detailed numerical models as a virtual *in silico* representation of the tissues/scaffolds/bioreactors can be advantageous. These models are designated digital twins and are developed with the motivation of providing a more profound characterization of the culture systems/scaffolds as well as optimizing stimulation parameters and predicting experimental outcomes while reducing the time and costs involved. The following work focuses on fluid effects, such as Wall Shear Stress (WSS) and Permeability, studying its distributions and changes according to different scaffold microarquitectures and dynamic culture conditions, for an iliac bone defect site treatment. For eight different scaffold geometries, with a graded and non-graded

(constant) porosity and different angular orientation in-between the filaments (0-30^o, 0-45^o, 0-60^o and 0-90^o), the Wall Shear Stress values pointed out the 30GRAD and 60NORM configurations, and Permeability values suggested that 30GRAD and 60GRAD were the best geometries, meaning that a graded porosity helped positively for a well-suitable iliac bone scaffold.

Resumo

A Engenharia de Tecidos Ósseos (BTE) surge como um campo de pesquisa biomédica focado na regeneração de defeitos do tecido ósseo usando *scaffolds* biodegradáveis, estruturas porosas que fornecem suporte mecânico e locais de adesão para as células ósseas proliferarem. Um dos objetivos da Engenharia de Tecidos (TE) é a cultura de células vivas dentro de dispositivos e *scaffolds* que criam um ambiente mimetizado de crescimento no tecido ósseo. Na cultura celular, destacam-se alguns aspectos: as interações das células com a membrana extracelular (ECM) envolvente, que modula a proliferação, diferenciação e funções metabólicas celulares; a influência de fatores ambientais, como estímulos mecânicos (por exemplo, efeitos induzidos por fluxo), elétricos e bioquímicos. Existe uma lacuna entre a arquitetura e a resposta biológica desses substitutos de enxertos ósseos porque cada construção deve atender a taxas específicas de reabsorção e biodegradação, crescimento ósseo e parâmetros de suporte mecânico, além de aplicar a composição e solubilidade do material aos pacientes e locais de implantação. Uma *scaffold* densa possui funções mecânicas superiores, enquanto uma altamente porosa melhora a entrega de células, ou uma permeável favorece o transporte de nutrientes e produtos residuais. A arquitetura ótima de uma *scaffold* aparece como um conceito relativo, uma vez que configurações diferentes aumentam e diminuem funções distintas.

Como complemento à pesquisa *in vitro* sobre a influência desses aspectos, o uso de modelos numéricos detalhados como representação virtual *in silico* dos tecidos/*scaffolds*/biorreatores pode ser vantajoso. Esses modelos são designados *digital twins* e são desenvolvidos com a motivação de fornecer uma caracterização mais detalhada dos sistemas/*scaffolds* de cultura, bem como otimizar os parâmetros de estimulação e prever resultados experimentais, reduzindo o tempo e os custos envolvidos. Esta dissertação foca-se nos efeitos induzidos por fluidos, como a Tensão de Corte (WSS) e Permeabilidade, estudando distribuições e variações de acordo com diferentes microarquitecturas de scaffold e condições dinâmicas de cultura, para o tratamento de um defeito no osso ilíaco. Para oito diferentes geometrias de *scaffold*,

com um gradiente ou porosidade constante, e diferentes orientações angulares entre os filamentos (0-30°, 0-45°, 0-60° e 0-90°), os valores de Tensão de Corte indicaram as configurações 30GRAD e 60NORM, e os valores de permeabilidade sugeriram que 30GRAD e 60GRAD eram as melhores geometrias, o que significa que uma porosidade com gradiente favorece *scaffolds* para aplicações do osso ilíaco.

Contents

List of Figures	xi
List of Tables	1
1 Motivation and Objectives	2
2 Introduction	3
2.1 Bone Tissue: Biology and Structure Overview. Related Diseases . . .	3
2.1.1 Biology of Bone Tissue	3
2.1.1.1 Bone Components	3
2.1.1.2 Bone Formation Pathways	6
2.1.2 Bone Structural Overview	7
2.1.3 Iliac Bone	8
2.1.4 Bone Related Diseases	11
2.2 State of the Art	12
2.2.1 Bone Tissue Engineering (BTE): Components, Challenges, In- novations and Drawbacks	12
2.2.2 Feature and Design Requirements of scaffolds	13
2.2.3 Scaffold materials and fabrication	16
2.2.3.1 Conventional Fabrication Methods	19
2.2.3.2 Additive Manufacturing Fabrication Methods	20
2.2.4 Cell Culture: Static and Dynamic Conditions	24
2.2.5 Dynamic Culture: Wall Shear Stress and Permeability	27
2.2.6 Mechanotransduction and BTE Scaffolds	31
3 Computer-Aided Engineering	32
3.1 Finite-Element Method	33
3.2 Computer-Aided Design and Simulation	34
3.2.1 Mesh Refinement	35

3.2.2	Computational Fluid Dynamics	36
3.2.3	Modelling the flow environment: Navier-Stokes Equations . . .	36
3.2.3.1	Laminar and Turbulent Flow Regimes	38
3.2.3.2	Modelling the mechanical environment: Wall Shear Stress	38
3.2.3.3	Modelling mass transport: Permeability	39
3.2.3.4	Wall Boundary Conditions	39
3.2.3.5	Solvers	40
4	Computational Methods	42
4.1	Computer Aided Design of Scaffolds	42
4.2	Computational Fluid Dynamics	46
4.2.1	Model Geometry	46
4.2.2	Applied Boundaries and Assumptions. Fluid Domain.	46
4.2.3	Mesh Convergence Study	48
5	Results and Discussion	50
5.1	Influence of different inter-filament orientation and porosity on velocity magnitude	50
5.2	Influence of different inter-filament orientation, porosity and flow velocity on Wall Shear Stress	52
5.3	Influence of different scaffold micro architecture on Permeability . . .	60
6	Conclusions	63
7	Future Work	64
	Bibliography	66

List of Figures

2.1	Hierarchy of structural components in a long bone. Adapted from [1]	7
2.2	Cortical and Trabecular Bone	8
2.3	MRI of pelvis and hip joint	9
2.5	Strain distribution in harvested and non-harvested iliac bone sites . .	10
2.6	Workflow of BTE strategy	12
2.7	3-D Printing with different a) Filament orientation and b) ofsetting layers with the same orientation, adapted from [2]	22
2.8	Solid-Form Formation techniques	23
2.9	Schematics of a spinner flask and a rotating wall bioreactors, respectively. Adapted from [3]	25
2.10	Schematics of a hollow fibre bioreactor. Adapted from [3]	26
2.11	From left to right, diagram of a direct and indirect perfusion bioreactors. Adapted from [3]	27
2.12	Shear Stress range for human cell lines	29
2.13	Morphology of cell attachment	30
3.1	Workflow in computationally-driven BTE applications	33
3.2	Structured and unstructured meshes	35
3.3	Defeaturing in mesh refinement	36
3.4	Wall Boundary schematics. adapted from [4]	40
4.1	Parameters used for CAD Design of Scaffolds	44
4.2	Computer-Aided Designs of Scaffolds	44
4.3	Model Geometry setup - VOI and Scaffold - for COMSOL Multiphysics software (version 5.2a, www.comsol.com , Stockholm, Sweden)	47
4.4	Mesh settings	48
4.5	Mesh Convergence Study	49
5.1	2D Plot Groups for velocity magnitude distribution	51

5.2	3D Plot Groups for Wall Shear Stress distribution	53
5.3	WSS Distribution over wall area, expressed as percentage, for 0-30° angular oriented scaffolds	54
5.4	WSS Distribution over wall area, expressed as percentage, for 0-45° angular oriented scaffolds	55
5.5	WSS Distribution over wall area, expressed as percentage, for 0-60° angular oriented scaffolds	56
5.6	WSS Distribution over wall area, expressed as percentage, for 0-90° angular oriented scaffolds	57
5.7	Permeability values with inlet flow velocities of 0.1 mm/s, 0.25 mm/s, 0.5 mm/s, 0.75 mm/s and 1 mm/s, for all configuration geometries of scaffolds	60
5.8	Pressure variation values with inlet flow velocities of 0.1 mm/s, 0.25 mm/s, 0.5 mm/s, 0.75 mm/s and 1 mm/s, for all configuration ge- ometries of scaffolds	61

List of Tables

2.1	Scaffold materials overview (adapted from [5])	18
2.2	Critical WSS values for seeded cells	31
2.3	Values for bone samples permeability's, according to several studies .	31
4.1	Parameters used for CAD Design of Scaffolds	43
4.2	Average of porosity in the models considered	45
4.3	Mesh features and quality parameters.	49
5.1	Statistical analysis for an inlet flow velocity of 0.1 mm/s.	58
5.2	Statistical analysis for an inlet flow velocity of 0.25 mm/s.	58

Motivation and Objectives

Science aiding science through interdisciplinary cooperation allows **Tissue Engineering** (TE) to be pictured as a mainstream, feasible approach to organ failure with high success rates rather than the ongoing risky organ transplantation [6]. Bone Tissue Engineering (BTE) is a clinical research field focused on replacing and healing damaged bone tissue using porous scaffolds that provide mechanical support, offering the adhesion sites for the bone cells to proliferate and differentiate [7].

The optimization of scaffold structure and architecture was performed through parametric design, allowing a patient-tailored approach for a personalized application. Scaffolds with an orthogonal grid-like pattern, layer angular orientations and varying pore dimensions were developed [8].

In bone scaffold-based strategies, fluid flow dynamics and oxygen concentration are parameters affecting cell proliferation, distribution, and activity. A drawback in the 3D-bone tissue engineering field is the lack of efficient vascularization strategies since a constant flow of oxygen and nutrients is needed to maintain *in silico* culture viability [9].

Numerical approaches maximize outputs of biological studies, as it allows a local or microscopic look, calculating beforehand mechanical deformations at the scaffold surface or fluid flow and nutrient transport within the architecture [10]. **Digital twins**, virtual representations of physical entities, can help optimize TE by linking physical laws, allowing iteration and personalization, integrating knowledge, and virtual testing before experiments [11]. **Finite Element Analysis** (FEA) software helps in designing and optimizing devices or processes by reducing prototypes and experiments, and **Computational Fluid Dynamics** (CFD) helps understand fluid flow in dynamic culture conditions (bioreactors) and its influence on scaffolds and bone growth [12]. This thesis work focuses on the fluid dynamics involved in 3D scaffolds applied for the iliac bone, studying the magnitude of velocity, wall shear stress and permeability among different architectures of geometry .

Introduction

2.1 Bone Tissue: Biology and Structure Overview. Related Diseases

2.1.1 Biology of Bone Tissue

Bone is a complex and dynamic organ continuously resorbed and new-formed, providing support protection for the soft tissues, storage for calcium and phosphates and harbour for bone marrow production. It is a mineralized connective tissue formed by a collagen-rich matrix and non-collagenous organic compounds, a heterogeneous compound comprising a mineral phase – bioapatite - and an organic matrix – type I collagen (90%), non-collagenous proteins (5%), lipid (2%), proteoglycans and water [13].

As a heterogeneous and anisotropic structure [14], bone is composed of an optimized irregular network of macrostructures - cancellous (comprising an average of 80% of bone tissue) and cortical bone (accounting for 20%) [15] -, microstructures (such as osteons and single trabeculae), sub-microstructures (lamellae), nanostructures (like fibrillar collagen) and sub-nanostructures (minerals and collagen molecules) all hierarchized and architected to fulfil the functional needs of each bone site.

2.1.1.1 Bone Components

Osteoblasts

Osteoblasts are cuboidal and polarized cells along the bone surface (4-6% of resident bone cells) with functions of bone formation (forming a matrix substance – osteoid – containing collagen) and regulation of mineralization levels. They form tight junctions with adjacent osteoblasts and clusters within mesenchymal conden-

sations, depositing bone on other surfaces.

Osteoblasts are derived from skeletal stem cells, which timely synthesize bone morphogenic proteins (BMPs) and members of the Wingless (Wnt) pathways for the osteoprogenitor lineage to happen. Differentiation of osteoblasts requires the expression of specific genes, such as Runx2 (Runt-related transcription factors) and CollA1, for the proliferation phase to begin. Fully differentiated osteoblasts show alkaline phosphatase (ALP) activity – preosteoblasts – and its transition to mature osteoblasts occurs when there is an increased expression of osterix (Osx), that promotes producing and secretion of bone matrix proteins, like osteocalcin (OCN), bone sialoprotein (BSP) I/II, and collagen type I. Other factors such as fibroblast growth factor (FGF), microRNAs, and connexin 43 play roles in osteoblast differentiation [13].

Bone matrix is synthesized firstly with the deposition of organic matrix and then with its mineralization. In the deposition of the organic matrix, osteoblasts secrete collagen proteins, non-collagen proteins (OCN, osteonectin, BSP II, and osteopontin), and proteoglycans (decorin and biglycan). We can divide the synthesis process into one vesicular phase and one fibrillar phase. The vesicular phase happens with the release of matrix vesicles from osteoblasts membranes to bind proteoglycans and other organic components. The fibrillar phase occurs when structures of calcium and phosphate ions, formed by proteoglycans and phosphate compounds degradation, supersaturate. The rupture of nucleation products, hydroxyapatite crystals, cause spreading through the bone matrix.

Bone Lining Cells

Flat-shaped osteoblasts that do not suffer resorption or new tissue formation. Its role relies on secretory activity according to physiological needs and on providing a physical interface between osteoclasts and bone matrix, being osteoblasts precursors and bone anabolic agents.

Osteocytes

These abundant and long-living cells constitute 90-95% of the total bone cells. Derived from skeletal stem cells lineage through osteoblast differentiation, they are located within the lacunae surrounding the bone matrix, and their cell bodies undergo cytoplasmatic processes forming a lacunocanalicular system. Neighbouring osteocytes are connected by gap junctions, facilitating the transport of small signalling molecules (prostaglandins) and nitric oxide and with the nearby vascular system, providing oxygen and nutrient achievement. Osteocytes play a mechanosensory

role, detecting mechanical pressures and loads and helping bone adaptation. They produce sclerostin, which regulates osteoblasts production. Their apoptotic process has been discovered to be a chemotactic signal to osteoclastic bone resorption as osteoclasts engulf them [13].

Osteoclasts

Osteoclasts are large, multinucleated cells responsible for bone resorption. Once attached to the bone surface, mononuclear hematopoietic progenitor cells express receptor activators of NF-kappa B (RANK) and interact with supporting cells expressing RANK ligand (RANKL). Osteoclast-specific transmembrane protein (DC-STAMP) and dendritic cell-specific transmembrane protein (OC-STAMP) trigger this process, capacitating osteoclasts for generating new osteoclasts by fission.

Osteoclasts are responsible for resorption products' attachment, resorption, and release. Attachment sites called podosomes (formed by the vitronectin receptor $\alpha_3\beta_3$ integrin and arginine-glycine-aspartic acid - RGD - sequenced in bone matrix proteins) create an actin-rich ring-like sealing zone that surrounds and isolates the resorption lacunae, allowing osteoclasts motricity across the bone surface by detaching and reattaching to the bone surface. These lacunae are acidified to dissolve bone minerals (bioapatite) and matrix proteins by carbonic anhydrase II. Cellular equilibrium is maintained by passive chloride-bicarbonate exchangers and chloride ion channels (CLC-7)

Extracellular Bone Matrix (ECM)

The bone's basic building block is the mineralized collagen fibril, composed mainly of a three-dimensional matrix of the fibrous protein collagen. Different levels of the organization are presented and are the basis for each differentiation process in various bone tissues.

ECM is a complex framework that brings homeostasis and mechanical support to the bone matrix, composed of inorganic salts (predominantly phosphate and calcium ions) and collagenous proteins (collagen type I, mainly) as well as non-collagenous proteins (osteocalcin, osteonectin, osteopontin, fibronectin, sialoprotein II, BMPs, and growth factors). The resulting structure allows the deposition of hydroxyapatite crystals and grants stiffness and resistance.

Bone remodelling is closely related to bone matrix proteins that interfere with the bone cells' activity. Adhesion molecules, like integrins, interact with bone cells via osteoblasts, and herein osteoblast organization on the bone surface and osteoid

synthesis are maintained. Osteoclasts function is also mediated through interaction with the bone matrix. A non-organized pericellular matrix involves the osteocyte cell body, and fibrous structures ensure its mechanosensitive function, as well as a fluid flux movement that allows bidirectional solute transport and, therefore, the signalling pathways and communication among bone cells [13].

2.1.1.2 Bone Formation Pathways

Bone mineralization

The deposition of osteoid is followed by calcium-phosphate mineralization, although this deposition and attachment processes are poorly known. It comprises a rapid initiation phase controlled by non-collagenous proteins osteoblasts-produced (osteocalcin, MEPE, PHOSPHO-1, alkaline phosphatase) and later secondary mineralization controlled by later osteoblasts and osteocytes proteins (DMPI, MEPE, ectonucleotide pyrophosphatase/phosphodiesterase, PHEX). Along gradient mineralization, bone matrix maturation is followed by a more ordered structure with crosslinked and compact collagen fibres, incorporation of carbonate in the bioapatite lattice, and less water content. Bone remodelling influences the level of mineralization. High bone remodelling rate results in lower mineralization since the second mineralization phase of the basic multicellular units (BMU) stops. When bone remodelling slows its rate, more bone content reaches its maximal mineralization state.

Bone Homeostasis and Bone Remodeling Process

Gradual renewal of cortical and trabecular bone happens on different surfaces. Bone remodelling comprises three phases: osteoclasts resorption (after an activation phase), transition to new bone replacement (with the formation of basic multicellular units), and new bone formation. Overall interactions between local and systemic factors assure bone cell formation, proliferation, differentiation and activity. Local factors include autocrine and paracrine molecules such as GFs, cytokines and prostaglandins, and bone matrix factors during resorption. Systemic factors include parathyroid hormone (PTH), calcitonin, 1,25-dihydroxy vitamin D3 (calcitriol), glucocorticoids, androgens, and estrogens. Increased levels of osteoporosis and bone loss with age are related to the estrogen decrease during menopause, inhibiting osteocyte and osteoblasts apoptosis that conducts to bone homeostasis.

Basic multicellular units (BMUs), formed by osteoclasts and osteoblasts, are temporary structures that form a remodelling compartment (possibly related to

bone lining cells on the bone surface) and communicate with the osteocytes in the bone matrix. Bone resorption occurs in the osteoclasts cell body, then a transition/reversal phase, and finally, the formation through osteoblasts. Among these phases, there are direct and indirect communications, forming the coupling mechanism that releases stored factors, within the bone matrix, during resorption.

2.1.2 Bone Structural Overview

Bone collagen fibrils are structured at a crystalline level with orthotropic symmetry, wound together in a triple helix. The mineralized collagen's building block is organized in layers, confirmed using three-dimensional electron tomography, with crystals traversing across the fibrils [16]. During the first stages of mineralization, this layered matrix limits crystal growth and fixates them along the fibrils. With continued growth, there is a compressing of the triple-helical molecules and a finalized joint phase. The interface between the mineral phase and the protein matrix shapes crystal growth and changes compressive and shear behaviour from externally applied loads. Fibril array patterns have great diversity. Parallel-fibered bone disposes of fibrils parallel to the bone axis, leaving big spaces filled with cortical bone and mineralized and stiffened bone surfaces, commonly seen in tendons attachment sites. Internal modelling of a bone done by osteoclasts comprises a phase of excavating of mineralized surfaces, cement deposition (osteoblasts function) and layering of lamellar bone. A small capillary-like channel is left at the centre, housing osteocytes that remain within the material. This whole cylindrical structure contains elongated pores and is called the osteon [17] and constitutes the majority of cortical bone.

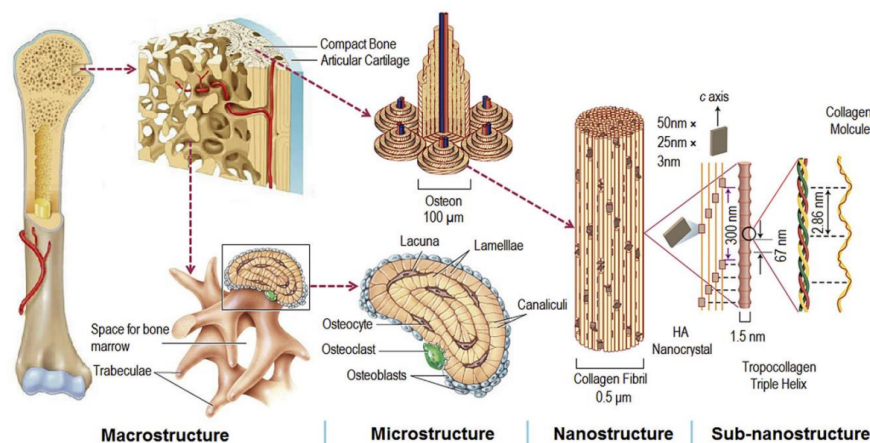


Figure 2.1: Hierarchy of structural components in a long bone. Adapted from [1]

Porosity

Osteocytic lacunae constitute bone porosity, a few millimetres sized canals that accommodate osteocytes, canaliculi in between with dimensions less than micrometres, and large diameter Haversian/Volkmann's canals, the central porosity portion of bone tissue. The osteocyte lacunae are strongly anisotropic in shape, changing in thickness and density with age increasing (approximately 30% more significant in younger ages [18]) [19]. The mechanical properties of cortical and cancellous bone rely on its porosity and thickness, meaning that an increased porosity is linked to increased fracture risk. In contrast to planar arrays of *lamellae*, osteonal bone remains attached after massive fracture behaviour, and wound healing happens if the two broken segments are nearby. Otherwise, a non-union fracture occurs, one of the BTE efforts to provide healing and new-tissue development.

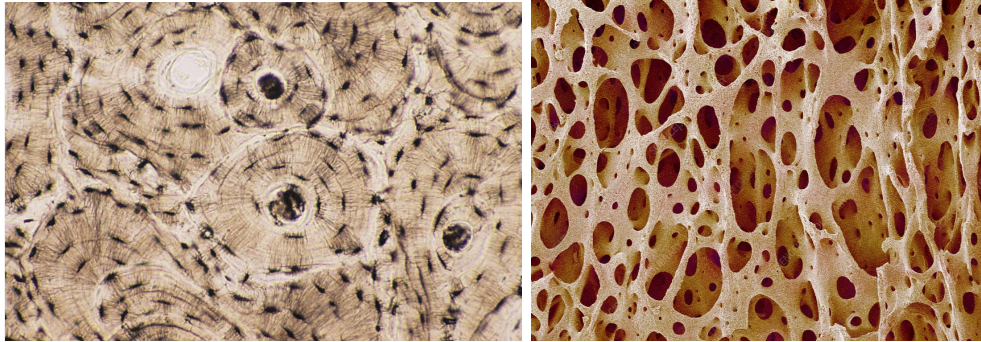


Figure 2.2: Cortical and Cancellous Bone, respectively. Adapted from [20] [21]

The spaces between the trabeculae in the trabecular bone are filled with either red bone marrow or yellow bone marrow, depending on the type of bone. Due to the differences in configuration and function of these two types of bone tissue, they possess different porosity (trabecular bone is 50-90% porous whereas cortical is only 10%) and different ultimate compressive strength (cortical bone can have up to 10 times higher compressive strength than trabecular bone) [22].

2.1.3 Iliac Bone

The iliac crest has a large amount of red bone marrow; thus, it is a "gold standard" site from bone marrow harvests to collect stem cells used in bone transplantation procedures. From orthopaedic and trauma surgery to reconstructive surgery or oral and maxillofacial surgery (filling in large osseous defects caused by periodontal disease, excess bone resorption and followed tooth loss), bone grafts provided by the iliac crest have a collection of well-suited properties, such as fair bone quantity (cancellous bone, cortical and vascularized graft, as seen in the figure 2.4) that combine

structural support with growth factors and progenitor cells [23].

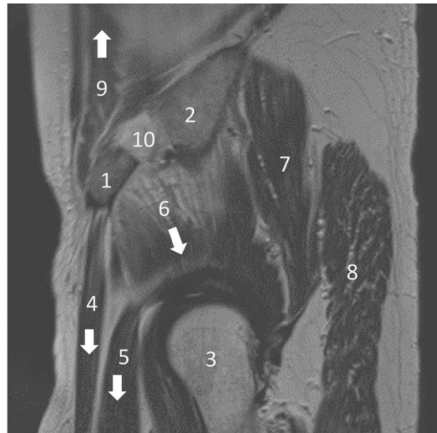


Figure 2.3: MRI of a pelvis and the hip joint in T2 sagittal reconstruction, with arrows showing traction of muscle forces responsible for fatigue fractures: 1-ASIS; 2-Iliac crest; 3-femoral head; 4-sartorius muscle; 5-femoral rectus muscle; 6,7,8-minor, medium and greater gluteal muscles; 9- abdominal muscle; 10- harvest bone site. Adapted from [24]

The current standard of treatment of bone defects concerns biological stabilization with fixation devices and artificial implants. Healing bone tissue is based on bone grafts and substitutes, restraining therapies because of the body’s immune response, disease transfer, infection or stress shielding. Hematoma, blood loss, infection and neurovascular injuries occur in up to 39% of cases, and chronic pain, cosmetic deformity and high probability for subsequent fracture motivate new therapeutic solutions. Regarding iliac bone harvesting, complications such as donor site pain, gait disturbance, numbness and fatigued fractures have to be accounted for to prevent complete incapacity or surgical treatment re-insurgence [25].

The iliac bone restoration procedure relies on standardized treatments such as xenografts (harvesting from non-human organisms), cancellous allografts (harvesting from another human body organism) and autologous rib transplantation (transplanting a patient’s healthy osseous tissue from one area to another), filling the defect gaps with plate fixation. These anatomically shaped low-profile plates and cortical screws aim to prevent fatigue fractures when the harvest site is relatively small and posterior to the ASIS. The force flow along the iliac crest to the posterior iliac wing is interrupted when the gap is created, and stress peaks posterior to the harvest site arise (as seen in the figure 2.5). Once the gap increases, there’s an increased risk of herniation of visceral organs due to the proximity of abdominal muscles.

Post-procedural complications can happen, with 0-4% of probability. In 2/3 of

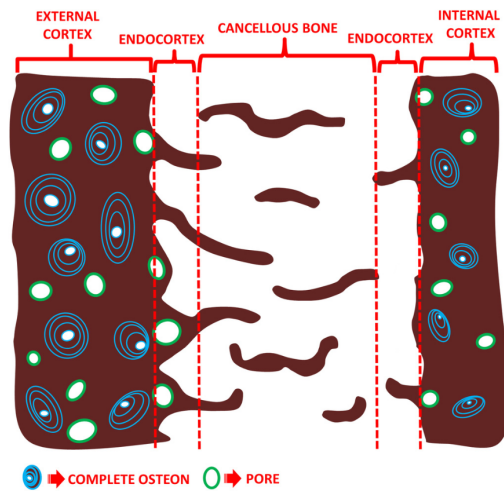


Figure 2.4: Iliac Bone schematics. Adapted from [23]

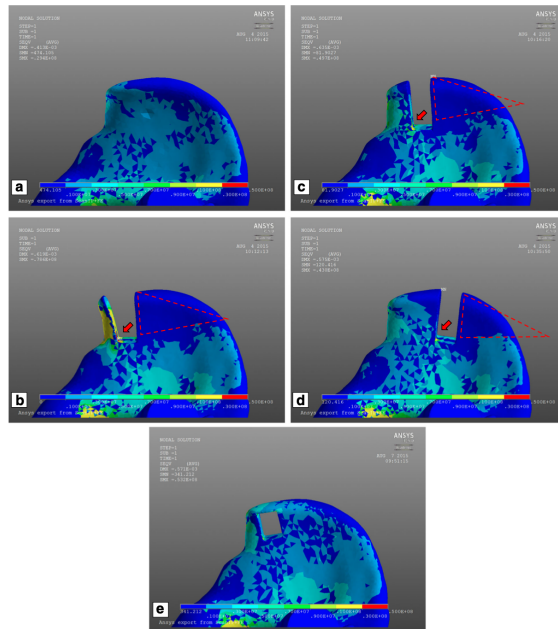


Figure 2.5: FEA results of stress distribution (a) without bone graft harvest and (b)(c)(d)(e) for four different sizes of harvesting bone grafts. Adapted from [23]

the cases, fatigue fractures of the anterior superior iliac spine (ASIS) after harvesting the anterior iliac crest take place, and a stabilization surgery to relieve postoperative fractures and pain (in most of the cases, caused by contraction of the attached pelvis muscles, sartorius and tensor fascia) happens in 16.6% of the cases. The purpose of this work aims to fill up these complications , with a Tissue Engineering.

2.1.4 Bone Related Diseases

In fracture healing, calcium homeostasis, and mechanical adaptation of bone structures, flaws in bone resorption and formation can result in various diseases [26].

Osteoclasts express and release lysosomes and proteolytic enzymes, which degrade collagenous bone components. An uncontrolled increase of osteoclast formation and activity can cause osteoporosis, caused by the imbalance in resorption and formation of bone tissue, conducting in decreased bone density and bone fractures. Some pathologies include bone metastases (abnormal osteoclast genesis results in periarticular erosion), inflammatory arthritis (resulting in osteolytic lesions), osteopetrosis (decreased bone resorption that causes accumulation of bone mass) and degenerative diseases (such as osteoarthritis and spondylosis)

Bone loss also occurs with ageing, being prone to infections (osteomyelitis, as an example) affecting both cortical and cancellous bone. Cortical bone's increased porosity is mainly due to increasing Haversian canal diameter and lowering of its density [27]. Several studies have shown that a negative balance in bone remodelling is caused by an increased resorption depth and/or decreased wall width.

2.2 State of the Art

2.2.1 Bone Tissue Engineering (BTE): Components, Challenges, Innovations and Drawbacks

Bone Repair and regeneration, the focus of BTE strategies, relies on four core components: **cells**, **growth factors**, **biophysical signals** and **scaffolds**.

In combination or individually, diverse strategies are engineered as alternatives to standard treatments. Cell therapies include mesenchymal cell injection or delivery, growth factors are implanted at supraphysiological doses to accelerate bone repair, biophysical signals employ physical and mechanical stimulation to facilitate regeneration, and scaffolds provide the framework for the fractured sites and harbour for cells at the healing zone.

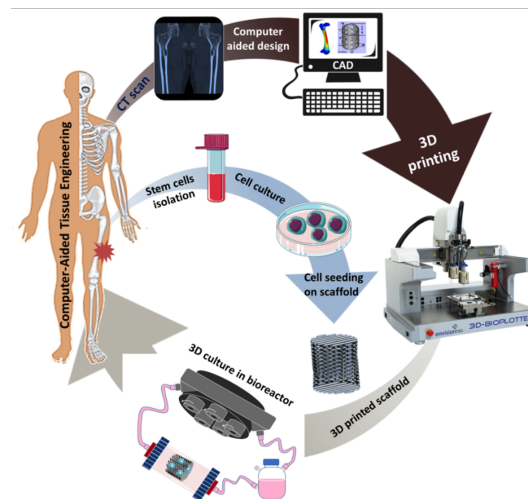


Figure 2.6: Workflow of BTE strategy. Adapted from [28].

Mesenchymal stem/stromal cells (MSCs) are adult multipotent cells capable of differentiation. From the vast availability to the fast expansion and differentiation *in vitro* capability onto various cell types (osteogenic, adipogenic and chondrogenic lineages), stem cells favour regenerative microenvironments with low immunogenicity and trophic and immunomodulatory activity. These cells are isolated from bone marrow, adipose tissue, muscle, periosteum, umbilical cord matrix, infrapatellar fat pad and synovial membrane.

Tissue engineering goal relies on surpassing surgical procedures by preparing materials that can be introduced to a specific defect and then remodelled by the patient's cells, using porous scaffolds to support and aid tissue repair and regeneration temporarily.

A scaffold is a matrix that stimulates attachment and proliferation of osteoinductive cells upon its surface, with functional and design requirements that must be met, such as biocompatibility with the cells attached, lack of toxicity and inflammatory responses, biodegradability for a safe substitution with osteoid deposition, mechanical properties to bear degradation processes, porosity levels and sizes for cell seeding and posterior nutrients and waste transfers, as well for angiogenesis, storability with no bioactivity loss, and allowed delivery of bioactive molecules/drugs. **Cell-based engineered bone grafts** appears as a histocompatible solution which delivers the patient's stem cells, growing an autologous cell population *in vitro* on scaffolds, achieving functionality for implantation. This *ex vivo* approach requires a precise mimicking of the internal micro-environment and the paracrine and autocrine signalling mechanisms for the desired cell differentiation, meaning that an inherent lack of bioactivity in the scaffolds can compromise the TE solution.

Scaffold-based techniques hold promising outcomes in the treatment of osseous defects, as the porous composite materials, subjected to physiochemical modifications, fulfil the functional needs of each particular bone. As for this *in situ* approach, the scaffold is implanted directly into the defected site, without initial cell seeding, depending on the body's intrinsic regenerative ability.[29]

2.2.2 Feature and Design Requirements of scaffolds

Modelling and producing suitable scaffold forms for BTE appliances endorses an understanding of native bone tissue composition and structure for an applicable selection of synthetic or bio-mimetic natural polymers for each treatment.

Therefore, construct architecture with scalable fabrication techniques are controlled and shaped in multiple length scales, with design considerations that can match disease modelling requirements. This section will overview design-based pathways for constructing implementation strategies and recapitulating physical structures and functional aspects of native bone tissue.

Analogous to a BTE scaffold, the bone ECM is made of a framework of crosslinked fibrils, layered, disposed and self-assembled, with in-between carbonated hydroxyapatite crystals. As previously explained, bone presents a varied density structure, with a dense outer region of cortical or compact bone, with an inner region of cancellous or spongy bone (comprising the trabeculae porous network).

Bio-compatibility, as the appropriate host response - body - to the design solution - scaffold - can be increased with surface characteristics that promote the

adsorption of desired proteins via receptors on their membranes or cell-binding capabilities within the material used. Chemical modification, however, can alter cellular adhesion through modification of surface hydrophilic portion, charge, roughness and overall chemical composition (different functional groups).[30]

Osteoinductivity, an intrinsic stimulation of osteogenesis, requires growth factors or solvable ions that allow differentiation of mesenchymal stem cells into osteoblasts. Moreover, osteoconductive materials are also required as they allow deposition on the surface and bonding to native bone tissue.

Mechanical properties are pivotal for a functional scaffold that can experience compressive loads without collapsing structurally but should match, preferably, native bone solutions, avoiding phenomena of stress shielding and consequent loss of bone density and weakening of surrounding tissues.

The biodegradation rate, synchronized with the mineralization of new tissue and deposition, should also match the gradual decrease of mechanical support and maintain overall functionality. The waste products should also be biocompatible with the BTE system.

Besides the bulk properties of the employed materials, the shape of the constructs needs to match the defect site geometries. Interior architecture has to create a growth medium of tissue and cells, with oxygen and nutrients supplied to provide the ingrowth of new tissue in an interconnected pore network. In the extent of vascularization inside the core of the scaffold, pore size is of critical importance because there is a controlled infiltration of new blood vessels and perivascular nerve fibres, as well as the seeding of osteoprogenitor cells. An increased innervation and the continued entrance of fluid onto the resident cells favour functional tissue regeneration, although jeopardizing the structure's mechanical properties.

The porosity of scaffold-tissue constructs is also a pivotal factor in the *in vivo* integration of a bioengineered bone graft, with a significant effect on the *in vivo* vascularization of tissue-engineered bone, mainly due to the high metabolic activity of bone cells, which require a highly efficient supply of oxygen and nutrients throughout a 3D porous scaffold. According to recent studies, new bone formation *in vivo* requires scaffold pore sizes of 300/400 μm , above which capillaries have been observed in newly formed bone. A pore size greater than 350 μm can enhance cell migration and angiogenesis.

Tailoring each design solution to a particular need restricts which properties are more needed. For large bone defects, mechanical properties gain importance, and

for small non-load bearing defects, minimally or non-invasive methods are preferred (injectable hydrogels, for example).

Scaffold Porosity

Porous structures are classified as closed or open pores, and the arrangement of unit cells can be stochastic and non-stochastic. Non-stochastic structures have a periodically regular form arrangement of unit cells and show higher mechanical properties than stochastic structures, where the unit cells are irregularly placed. The percentage of total void space is the **total porosity**, a factor that affects cell recruitment, attachment, and vascularization of the scaffold. The **open porosity** is the percentage of pores that are interconnected, affecting cell permeability and tissue infiltration, as well as molecular diffusion through the construct.

Three-dimensional unit cells can be designed computationally from the diamond lattice, face-centered cubic or body-centered cubic, some examples of orientated structures. A theoretical porosity can then be derived from structural parameters. Low porosity offers mechanical strength but lacks a reduced bone in-growth, promoting pore occlusion. [31] The pore size, as the diameter of the largest sphere that fits within a pore channel, affects cell infiltration, migration, proliferation, distribution, ECM deposition and distribution, nutrient, and oxygen exchange.

Localized and gradient porosity have been proposed to increase tissue specific growth during the regeneration process. This allows nutrient transport throughout the scaffold based on the scaffold and tissue architecture. [32]

Tortuosity

Quantification of twists and turns through a connected channel, expressed as the length of the entire channel divided by the shortest distance between starting and ending points Affects surface area, cell migration, delivery of nutrients and removal of waste.

Surface area to volume ratio

Ratio of total scaffold surface area to total scaffold volume, to be considered when defining cell seeding density and concentration of functionalization factors on scaffolds.

Swelling ratio

The ratio of wet mass or volume to dry mass or volume of a hydrogel. Swelling can affect delivery of growth factors or oxygen diffusion, leading to changes in cell

response, as well as affect cell attachment and proliferation. [32] [33]

2.2.3 Scaffold materials and fabrication

Osteoconduction, as the allowance of migration of mesenchymal cells, osteoblasts, osteoclasts, vascularization and stimulation of differentiation onto osteogenic cells, is a crucial factor that dictates successful scaffolding.

Synthetic and natural, biodegradable and non-biodegradable materials are used in the fabrication of these constructs, according to different methods, and show various responses as specific resorption rates, biocompatibility and surface reactivities. The choice of biomaterial and its fabrication strategy is dictated according to whether the material is meant to generate bone-like tissue *in vitro* before implantation or facilitate the formation of bone tissue at the defect site *in vivo*. A trade-off is needed regarding the materials on which the highly porous scaffolds rely. Ideally, these systems would be load-bearing once incorporated, but materials that are superior in terms of mechanical properties are often inferior in terms of biological compliance [34].

Polymeric scaffolds allow a controllable maneuver of physicochemical characteristics, enzymatic reactions, and allergic responses. Natural scaffolds can be cell-derived or tissue-derived, according to which material is seeded onto the matrix after a decellularization phase to avoid the immune response. They are composed of extracellular biomaterials which show osteoinductive materials (proteins, polysaccharides and polynucleotides), and they are employed in allogeneic and xenogeneic scaffolds, with the advantage of no additional surgery and no donor site morbidity but lacking in availability, mechanical properties, consistency and biodegradability.

Synthetic polymers present good mechanical properties and a controlled degradation rate but can leave an acidic microenvironment propensity to adverse tissue responses. They are constituted, among a vast diversity, of aliphatic polyesters such as poly(lactic-acid) (PLA), poly(glycolic-acid) (PGA), and poly(caprolactone) (PCL), and respective copolymers.

Ceramic scaffolds have superior mechanical strength than polymer-based constructs, lacking still in terms of tensile and torsion strength. Bioceramics provide high cellular adherence and proliferation. Calcium phosphate ceramics, for example, hydroxyapatite+ tricalcium phosphate as a combination of biphasic calcium phosphate (BCP) and amorphous calcium phosphate (ACP), improve bioactivity levels and modifiable mechanical strength levels, dissolution rates and biocompatibility in

vivo.

Composite scaffolds such as polymer/ceramic composites (with bioceramics such as CP, HA, PLLA- TCP with Poly(L-lactic acid)-, collagen, gelatin, and chitosan) have excelled in mechanical integrity properties and osteoconductivity.

Other combinations include collagen/bioglass nanocomposites, calcium coatings on metals, glasses, inorganic ceramics and organic polymers, collagens and silk fibres, and the addition of phosphorous or carbon and tantalum deposits on metals, which are a few examples of promising orthopaedic applications. Metallic scaffolds have introduced mechanically robust materials that could match hydroxyapatite (approximately 70% of bone mass) compressive strength, in the range of 500-1000 MPa, and bending strength, in the range of 115-200 MPa. However, they are non-biodegradable and prejudice bone functionality. Ideal solutions could rely on surface modifications or osteoconductive composite loaded with specific growth factors.

Table 2.1: Scaffold materials overview (adapted from [5])

Material Type	Advantages	Limitations	Examples
Natural polymers: Poly- saccharide Protein based	Biomimicry with ECM (are a component of ECM or have similar structure) Biocompatibility Biodegradability Little or none inflammatory response	Poor mechanical properties Potential immunogenicity (in some cases) Rapid degradation Batch-to-batch variability Lower bioactivity from non-human polymers	Hyaluronic acid (HA) Chondroitin sulfate (CS) Alginate Agarose Chitosan Collagen Gelatin Silk fibroin
Synthetic polymers	Consistent product characteristics Good biocompatibility Wide range of compositions and properties Versatility Ease of modification Low immunogenicity	Low bioactivity or inert for cellular interaction Possibility of undesirable or acidic degradation products	Poly(ethylene glycol) (PEG) Poly(ethylene oxide) (PEO) Polylactic acid (PLA) Poly(lactic acid-co-glycolic acid) (PLGA) Poly(ϵ -caprolactone) (PCL) Poly(vinyl alcohol) (PVA) Poly(L-glutamic acid) Poly(propylene fumarate) (PPF) Poly(N-isopropyl acrylamide) (PNIPAAm)
Bioceramics	Biocompatibility Bioactivity Mechanical strength	Brittleness Mimic mostly bone	Hydroxyapatite (HAp) ($\text{Ca}_5(\text{PO}_4)_3(\text{OH})$) Tricalcium phosphate (TCP) ($\text{Ca}_3(\text{PO}_4)_2$) Calcium silicate Bioactive glass (BG)
Metals and their alloys	Mechanical strength Biocompatible	Lack of biodegradability (in many cases) Risk of stress shielding Mimic mostly bone	Titanium Magnesium/Zinc
ECM-based materials	Similarity to the complex composition of ECM Bioactivity and tissue specificity	Poor reproducibility Limited standards for decellularization	Decellularized ECM Pulverized ECM particles for composite fabrication

2.2.3.1 Conventional Fabrication Methods

The advent of functionally tailored, biocompatible and biodegradable materials for use in regenerative tissue engineering has been the focus of research, with a broad of scaffold fabrication techniques and future trends in their development and clinical relevance.

Solvent Casting and Particulate Leaching (SC/PL) relies on a dissolved polymer in a volatile solvent, with a uniformly distributed porogen (organic compounds like gelatin and collagen or water-soluble inorganic salts). Once the solvent evaporates, the porogen stays in the polymer network, creating pores when leached in a porogen solvent. Varying salt/polymer ratio, particle size or porogen shape can result in a highly porous construct, however, with low control over inter-connectivity, lacking mechanical properties.

Melt Molding uses thermoplastic polymers, which melt in a mould structure to create the desired construct. Porosity is then introduced by merging other conventional methods such as **Gas Foaming** (blown gas to create void areas in the matrix) or **Thermally Induced Phase Separation (TIPS)** (converted polymer into a polymer-rich phase and a polymer-deficit phase).

Freeze-Drying consists of a dispersed polymer prepared with additives to be dissolved in organic or inorganic solvents. The solution is then mould-casted and frozen below its triple point (coexistence of three states of matter). Once its ice crystals sublime (in followed drying phases), a network of pores appears. Altering parameters of this operation can modify pore sizes, although associated with high production costs. **Sol-Gel Method** is mainly used in bioceramics and bioactive glasses production and is based on a colloidal state solution formed by the hydrolysis of inorganic or organic metal compounds, followed by dehydration or chemical stabilization.

Electrospinning is one of the most common strategies, consisting in the production of ultrafine fibres by charging and ejecting a steady steamed polymer melt or solution through a spinneret (under a high-voltage electric field) and solidifying or coagulating it to form a filament. The platform and the syringe pump are connected to opposite electric potential terminals. This potential difference is responsible for drawing the original diameter of the material, achieving several orders of magnitude. Once deposited onto the platform, it solidifies to form the desired filaments.

2.2.3.2 Additive Manufacturing Fabrication Methods

Large bone defects repairment can be achieved with additive manufacturing (AM), also known as solid free-form fabrication (SFF) or rapid prototyping (RP), technologies for materials processing and manufacturing methods that customize scaffolds, prototyping a multitude of internal architectures and pore size distribution.

The application of AM techniques consists of acquiring anatomical structure data to generate a three-dimensional computer-aided design (CAD) of the scaffold and the anatomical structure of the defect.

Material deposition methods divide AM into direct printing technologies, nozzle-based and laser-based systems. Fabrication of scaffolds by stereolithography (SLA), selective laser sintering (SLS), electron beam melting (EBM), fused deposition modelling (FDM), low-temperature deposition, and 3-D printing are some of the available methodologies. [35][34]

One big challenge in the bioengineering of clinically relevant size bone tissues relies on the transport of oxygen, nutrients and metabolic waste products. Additive manufacturing (AM) methods usually employ synthetic materials lacking bioadhesive sites, causing low cell attachment sites. Several approaches for enhancing cell adhesion have been used, such as coating scaffolds (with cell-binding motifs) or changing the porosity and fibre orientation. One drawback relies on the compromise between cell adhesion-promoting materials, and MSC condensation, needed for chondrogenic differentiation, that can be inhibited by surfaces that promote cell stretching upon their attachment.

Stereolithography (SLA) was the first laser-based system technology to appear and consists of a photosensitive liquid resin irradiated with UV light so that it can deposit a solid filament (sinter powdered material) over a moveable platform (layer by layer). As for powder bed fusion systems, techniques such as **Selective Laser Sintering, Selective Laser Melting, Direct Metal Laser Sintering and Electron Beam Melting** are available.

Fused Deposition Modelling is an AM technique in which thin thermoplastic filaments or granules melt by heating and are guided by a robotic device to generate the 3D object. The material leaves the extruder in a hot liquid form and solidifies upon cooling, layer by layer, maintaining a temperature just below the solidification point of the biomaterial. **Material Extrusion: Fused Filament Fabrication, Wet-Spinning Based Extrusion, Direct Writing.**

3-D Printing

3DP was initially developed at the Massachusetts Institute of Technology at the beginning of the 1990s and is based on the selective deposition of droplets of a binder material over a powder bed, using an inkjet head, merging the particles and forming a solid layer. After deposition, the build platform is lowered, a new layer of powder is placed over the previous one, and the entire process is repeated until a 3D object is built. The powder that remains unbound supports the material in the ensuing layers. The loose powder is separated in the end, revealing the formed object [36]. Sintering processes are sometimes used in a post-processing stage to improve the mechanical properties of the construct. In those situations, construct shrinkage is mentioned limiting the use of incorporated biomolecules.

3D printing consists of binding particles, and the powdery rough finish of the parts causes difficulties in removing trapped material in complex geometries. Another drawback is the need for more adhesion between layers compared to SLA, SLS and FDM techniques. As this method does not require heat, it incorporates bioactive molecules into the process. When polymer powders are used with organic solvents as binders, biocompatibility issues need to be considered, as well as adapting the printhead to withstand these solvents. The Bioplotter is an extension of 3DP, printing material processed either thermally or chemically. Bioprinting uses autonomous self-assembly and biomimicry for complete organ fabrication and building blocks for tissue formation.

The resources of 3DP allowed scaffold characteristics to be adjusted, by controlling process properties such as powder size, size distribution, roughness, shape, and wettability, as well as the chemical reactions between the powder and the binder.

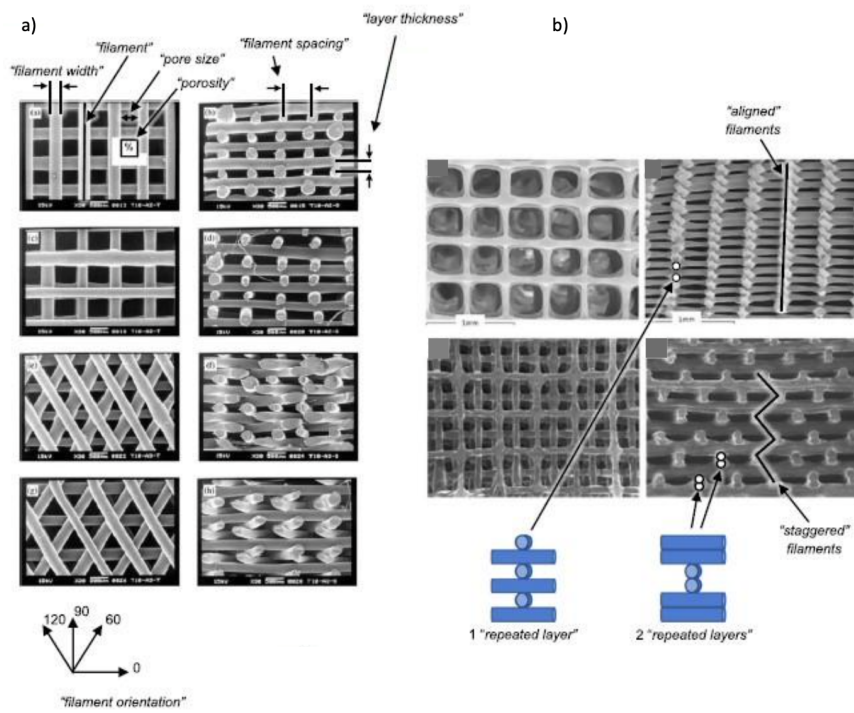


Figure 2.7: 3-D Printing with different a) Filament orientation and b) offsetting layers with the same orientation, adapted from [2]

2. Introduction

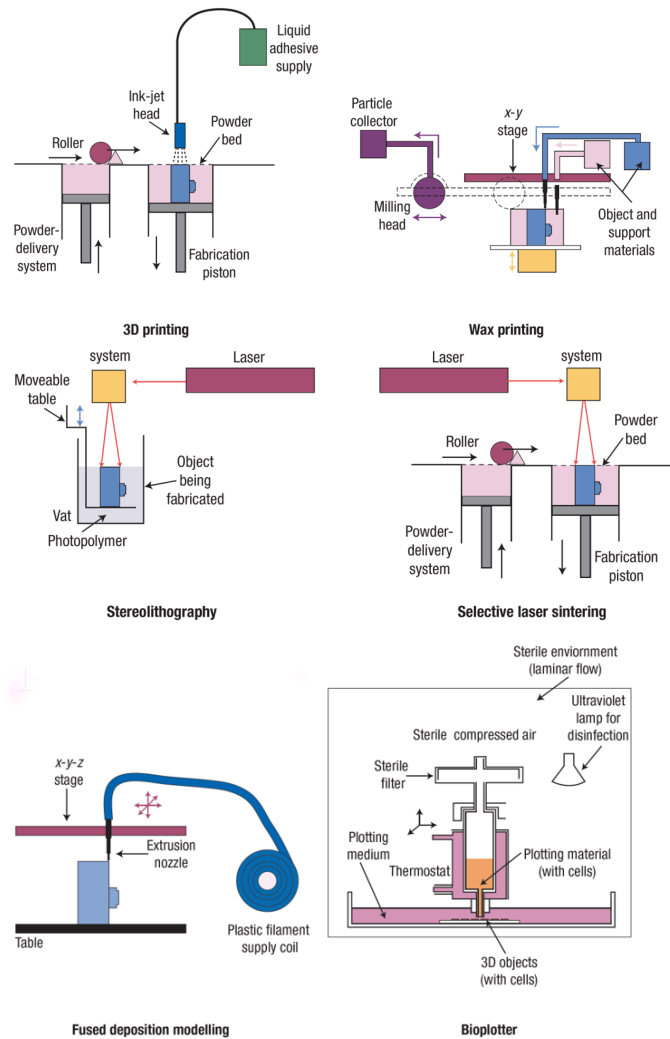


Figure 2.8: Solid-Form Formation techniques. From left to right, Printing-based systems (3D and wax printing), Laser-based systems (stereolithography and selective laser sintering) and Nozzle-based systems (fused deposition modelling). Adapted from [37].

2.2.4 Cell Culture: Static and Dynamic Conditions

Osteogenic preconditioning of cell culture, prior to the implantation *in vivo*, is shown to enhance vascularization and bone formation pathways at the recipient sites [38]. Culture conditions are divided in conventional/static or dynamic approaches. **Conventional techniques** for stem cell differentiation rely on soluble molecules inducing signals of a desired phenotype. These static conditions are diffusion-only dependent and cannot account for mass transfer (associated with poor nutrient diffusion) and cell culture growth, which leaves an uneven distribution toward the scaffold, going peripherally and leaving necrotic cores. **Dynamic conditions**, when culturing seeded scaffolds *in vitro*, surpass the static conditions drawback, incorporating systems of controllable diffusive exchange that provide *in vivo*-like mechanical and chemical cues to the cells, with perfusive or convective currents delivering nutrients and stimulating cultures within the scaffolds (pressure drop and shear stress, as an example). In large bone substitutes, nutrients cannot be delivered to the centre of the scaffold, and waste cannot be removed, leading to cell necrosis. Contrary to static culture, bone substitute cultures can enable real-time cell culture monitoring and provide, under dynamic cell culture conditions, an early overexpression of osteogenic markers and increased waste removal, allowing nutrient transport and osteogenic stimuli toward cells [39]. **Bioreactors** can mimic the physiological microenvironment of cell culturing by augmenting mass transport through media convection, proliferating nutrient delivery, and mechanically inducing shear-flow stress stimuli, inducing bone tissue mineralization. Osteogenic differentiation, seeding efficiency and homogeneity of cell spreading are the overall advantages of this realistic-type system.[3]

The bioreactor research on operating conditions uses the factors available - fluid flow, nutrient distribution and flow shear stress - to create reproducible and functional protocols for BTE applications. Potentially bone substitute cultures like spinner-flask, rotating wall, perfusion and hollow-fibre bioreactors have shown promising outcomes in developing functional grafts.

Spinner-flask bioreactors

Setup formed by a stir bar, a magnetic or rotating paddle, that provides a convective fluid flow irrigating the fixed scaffolds inside a lid. ECM deposition and cell differentiation are noted in the construct periphery, but there is an irrigated volume compromise, as the flow cannot penetrate the interior of large scaffolds. Modelling tools around spinner-flask simulations performed by Freed et al. [3] showed that

this mass transport constraint caused inhibition of chondrocytes proliferation rate on thick biodegradable polyglycolic acid (PGA) scaffolds. *In vitro*, spinner-flasks perform better than static cultures and rotating wall bioreactors with disc-shaped scaffolds (diameters of 4-10 mm). According to various studies, fluid agitation in 3D systems reduces mass transfer constraints due to concentration gradients at the medium interface boundaries (fluid construct).

Rotating wall bioreactors

The structure is made of two concentric cylinders rotating, with cultured cells and media in between. The inner cylinder is oxygenated and covered by a membrane that delivers oxygen to the media, microcarrier cultures (forming tissue aggregates in the chamber) and scaffolds. Rotation speed runs along specific values matching conditions for free-fall of scaffolds, therefore inducing low shear stresses that could provide suboptimal mechanical stimulation. Lappa [3] developed a comprehensive model comprising tissue-growth rate, nutrient concentration and flow profile to assess the later stage of ECM expansion of cartilage constructs cultured in a rotating wall bioreactor. The predictive ability of this model concluded that size-increased scaffolds had increased growth in lower edges, with mass transfer and shear transfer enhanced.

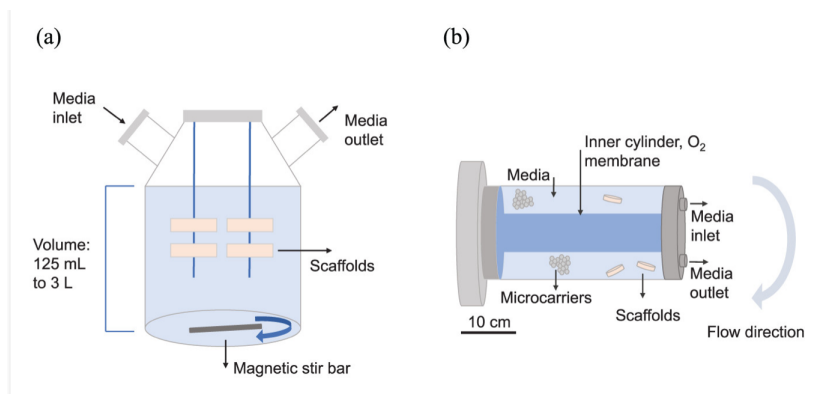


Figure 2.9: Schematics of a spinner flask and a rotating wall bioreactors, respectively. Adapted from [3]

Hollow fibre bioreactors

Bioreactor consisting of fibres through which the flow medium is perfused, allowing cells to seed in its outer surface or the matrix. The fibres' resemblance to capillaries facilitates angiogenesis. Cell-oxygen requirements and permeation were studied, as well as the minimal adequate amount of BMP-2 ([40]), as indicators of this configuration validity. Studies have found that enhanced mass transfer was verified, even submitting the cells to excessive shear stress values.

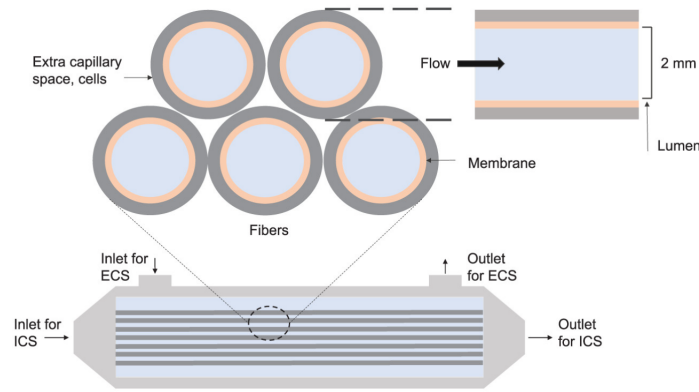


Figure 2.10: Schematics of a hollow fibre bioreactor. Adapted from [3]

Perfusion bioreactors

Model in which the medium is pumped through a chamber, with direct perfusion configuration with fluid flow through the scaffold, and indirect with the fluid flow around the scaffold. Both systems have very positive outcomes in the quality of tissue formation after implantation *in vivo* and oxygen distribution throughout the scaffold (although reduced in the presence of media convection). Mechano-regulated osteogenesis was studied by Guyot et al. [41], analyzing the deformations upon different positioning of the scaffold subjected to different flow rates. Small strains were visualized, but osteogenesis was induced, indicating that shear stresses formed in the chamber mechanically stimulated cell culture growth.

Perfusion offers benefits as fluid is forced through the entire construct, creating a more homogeneous microenvironment rather than improving convection at the surface of the scaffold [42]. The nutritional supply and removing of waste products is enhanced with perfusion regimes, because it mimicks bone deformation strains as the result of motricity [43]. Regarding flow application in culture medium, various studies suggest that regimes like pulsatile or oscillatory flow patterns upregulate osteogenic growth [34]. Rest insertion (or low flow) periods between bouts of higher shear stress (for various flow types) have been explored by several authors to negate cellular desensitization and appear to lead to a considerable enhancement of gene expression.

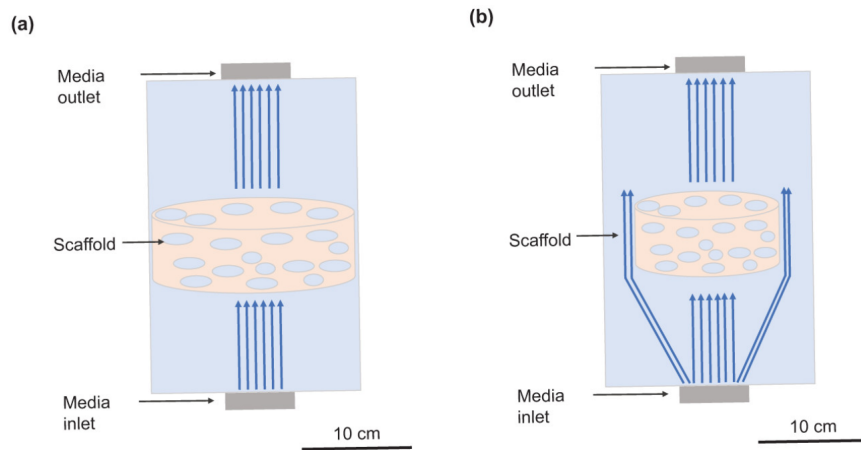


Figure 2.11: From left to right, diagram of a direct and indirect perfusion bioreactors. Adapted from [3]

2.2.5 Dynamic Culture: Wall Shear Stress and Permeability

Bone tissue engineering aims to provide a means *in vitro* of tissue development that fastens healing time *in vivo*. Therefore, fluid shear stress, cellular deformation and osteogenic differentiation act in a hierarchical cascade of external cues for new tissue growth. **Mechanotransduction** is understood as incorporating biological signals from cell-applied physical forces. As the research into the pathways involved in this mechanism is still active, theories based on the nature of the responses are: i) a regulation of stretch-activated ion channels, with ions fluxing in and out of the cell via force-induced changes in the plasma membrane; ii) the deformation of the cytoskeleton by extracellular matrix ligands with integrins, which are the point of bonding responsible for the transmission of an external force across the plasma membrane into the cell, triggering responses through internal organelle movement. Biomechanical stimuli comprise strain, caused by physical deformation, and fluid shear stress, generated by compression and tension under loading of the interstitial fluid movement through *lacunae*.

Wall Shear Stress

Fluid-induced wall shear stress is created by fluid movement tangential to the face of a surface, linearly proportional to the velocity gradient perpendicular to the shear plane. The governing equation is written as:

$$\tau_{ij} = \mu \left(\frac{\partial v_i}{\partial x_j} + \frac{\partial v_j}{\partial x_i} \right) \quad (2.1)$$

- where τ_{ij} = shear stress on the i^{th} face of a fluid element in the j^{th} direction; μ = fluid viscosity; v_i and v_j = velocity in the i^{th} and j^{th} directions, respectively; x_i and x_j = the i^{th} and j^{th} direction coordinates, respectively. Wall Shear Stress depends on fluid velocity, and this velocity is linked to the flow rate selected on the direct perfusion bioreactors. If the inlet flow rate is too low, mass transfer limitations cannot be overcome, and nutrients cannot be present at the centre of the scaffold. If the inlet flow rate is too high, the velocity inside the pores is consequently also too high, and the seeded cells in the scaffold could be dead or detached.

Under natural conditions, bone homeostasis and remodelling are regulated by matrix strain and interstitial fluid movement caused by physical activity. Under culture, pluripotent stem cells are differentiated (onto osteoblast phenotypes or hematopoietic, endothelial and cardiac cell lineages) upon specific wall shear stress' ranges. Reports suggest that 0-30 mPa stimulates the overall biological activity of mesenchymal stromal cells (MSCs), in the range of 0.11–10 mPa stimulates osteogenic differentiation, and in the range of 0.55–24, mPa stimulates the mineralization process of bone cells.

A nonuniform shear stress distribution will result in heterogeneity of cellular responses, thereby changing the porosity, geometric architecture of scaffolds and inlet perfusion conditions, and extent of the biomechanical stimuli experienced by the controlled cells. Critical shear stress levels - shear stress level required to remove 50% of attached cells - vary on surface properties and cellular characteristics and frequently happen for values >1 Pa [34].

Fluid pressure and wall shear stress impact the nitric oxide levels within the scaffold, which leads to a mechanical stimulus on cells [44]. Also, several studies conducted mechanical induction of osteogenesis on 2D flow systems, and reported osteoblast precursors activity at shear stresses of 2Pa, by upregulating osteogenic markers, such as collagen type 1 (COL1), osteocalcin (OCN) and alkaline phosphatase (ALP) after 3 days of continuous perfusion cultures [45]. Moreover, studies revealed MSCs undergoing osteogenesis solely by mechanical stimuli, at ranges of 0.4-2.2Pa.

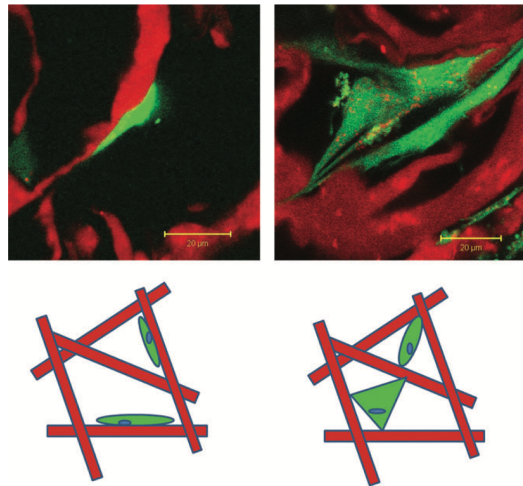


Figure 2.13: Top: fluorescent microscopy images showing cells attached either predominantly flatly to collagen struts (left) or in a bridged manner (right). The collagen structure is depicted in red, and the cell cytoplasm in green. Adapted from [34]

Different cell types and culture conditions, according to several studies, have revealed an essential role of shear stress through different ranged values for osteogenic lineages of differentiation, showing that from a range of 0.1-0.5Pa, or from values as high as 2Pa, there is an upregulation of genes or protein expression, such as COX-2, Runx2, BMP2/7 and Sox9. [34]. Mineralized matrix production can be achieved in the range 1×10^{-4} to 1.2Pa. Ideally, vascularization of constructs should happen before the implantation *in vitro*, avoiding nutrient deprivation by the host if there is a substantial growth of tissue *in vitro*. Mechanical stimuli can enhance the differentiation, such as dynamic compressive loading for cartilage formation, uniaxial strain or axial compression/tension and torsion for ligament growth. Successful vascularization, according to studies, has occurred for values above 1.2Pa. The following table summarizes WSS values under different studies:

WSS (mPa)	Effect	Author
1.5-13.5	Stimulation	Raimond et al (2002) [46]
0.05	Proliferation	Cartmell et al. (2003) [47]
1	Differentiation	
57	Apoptosis	
4.6	Stimulation	Raimond et al (2006) [48]
14-25	Differentiation	
56	Cell wash out	

Table 2.2: Critical WSS values for seeded cells, adapted from [49]

Permeability

Permeability refers to the ability of fluid and nutrients to flow through a material and is important for maintaining the health and viability of cells and tissues. A high permeability ensures adequate delivery of nutrients to cells and removal of waste products, which can be critical for the success of tissue engineering. The following table summarizes permeability values under different studies:

Authors	Experiment	Permeability (m^2)
<i>Grimm and Williams (1997)</i> [50]	Human trabecular bone from fresh-frozen calcanei of cadavers	$(0.4-11)*10^{-9}$
<i>Nauman et al. (1999)</i> [51]	Trabecular bone samples from human vertebral body	$(1.5-12.1)*10^{-9}$
	Trabecular bone samples from human proximal femur	$(0.01-4.7)*10^{-9}$
<i>Rothweiller et al. (2022)</i> [52]	Cortical bone samples from iliac bone	$(0.17-3.57)*10^{-13}$

Table 2.3: Values for bone samples permeability's, according to several studies

2.2.6 Mechanotransduction and BTE Scaffolds

When bone cells are attached on a solid substrate - scaffold -, their functionality depends on the biomaterial's topography, degradation rate, or chemical characteristics. As it strongly influences the adsorption of molecules secreted, to form a viable extracellular matrix and activate bone cell surface receptors and intracellular proteins responsible for signal transduction, mechanotransduction induced via cyclic stretch to create cytoskeleton tension has revealed that gap junctional communication between osteoblasts increased, and pulsating fluid flow appeared as a strong osteocyte stimulator [53], showing that a proper culture system enhances nutrient transport and mechanically stimulates the seeded cells.

Computer-Aided Engineering

Digital twins can be seen as an engineering strategy with the following advantages in TE: i) linking physical laws and process parameters describing an experiment in a computational system, ii) allow the increase in knowledge about that experiment through an iterative fine tuning process; iii) allow a decrease in development costs for experimental design; iv) is compliant with the development of patient personalized solutions; v) facilitates the integration of acquired knowledge and improvements to the digital twin during the lifecycle of a product; vi) make possible the evaluation, screening, and virtual testing of new configuration and settings prior to experiments.

One way to classify digital tools is according to the modelling method supporting the model. Mechanistic models are developed based on concepts and hypothesis informed by biological knowledge and insight, with its parameters having a physical meaning. However, they may have a higher cost of development, be more difficult to parametrize, and be generally harder to compute in real-time, which can frequently be a requirement for digital twins. Additionally, if the complexity of the biological processes is too high, or the understanding of the process is too limited, a fully mechanistic model will not be achievable. Conversely, data driven models are developed only with experimentally generated evidence. Due to this black-box nature, they provide less insights into the system, and are more straightforward to develop. In situations where data-logging is faster than its analysis, they provide a good basis for prediction and control. Nevertheless, there might be some reluctance in using these models in clinical settings, as results from data-driven models can often not be extrapolated to cases outside the scope of the training data. Alternatively, hybrid strategies combining both models could provide a more capable framework.

Changing scaffold structure and porosity imposes renewal of experimental processes and calculating optimal growing conditions through simulations of *in vitro* culture environment saves time with numerical methods that apprehend a micro-

fluidic environment.

Computational fluid dynamics are used to understand fluid flow within bioreactors and, therefore, the constructs structures, allowing us to bring a comprehensive network into the effect of fluid-induced stress onto porous scaffolds and bone growth. Integrated research in biomedical sciences applied to bone tissue engineering has developed computational models based on physical, mechanical and/or experimental data to minimize variability and optimize the overall output of applications. The following chapter will cover computing tools for product design and *in vivo* study of processes which assist the modelling of complex biological systems, scaffolds and bioreactors.

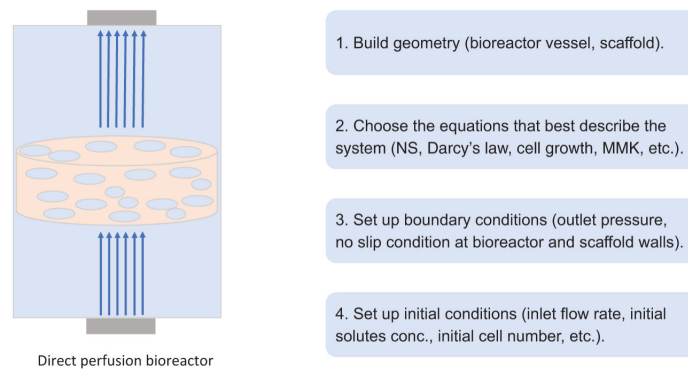


Figure 3.1: Workflow in computationally-driven BTE applications

3.1 Finite-Element Method

Describing a system's behaviour requires an understanding of its physical description. Therefore it can help predict, optimize and control a design or operation of a given process/device.

The Finite-Element Method (FEM) is a discretization procedure of continuum mechanics problems displayed as mathematically defined statements. The continuum mechanics, such as conservation laws, is divided into a finite number of parts (elements), with specified behaviour by a finite number of parameters, and the solution of the system is the assembly of its elements. These numerical models are an approximation associated with an error of accuracy, the truncation error, that approaches to zero as the model becomes stable and consistent.

For space and time-dependent problems, these discretized equations are partial differential equations, and the dependent variables of a given system represent the solution. For time-independent, stationary problems solution is found in one time-

step, following a number of linear equations, depending on the number of studied variables.

Boundary Conditions and initial conditions define the physical state of the mathematical system and conduce to a converged solution. Through a computational mesh, test functions are locally defined in each mesh element, forming shape functions with associated weights and degrees of freedom (DOFs).

The workflow involved in FEA begins with a preprocessing of the geometry upon analysis, with repairing and defeaturing of 3D surfaces that can result in an undesirable concentration of elements, such as short edges or slender surfaces. It is mandatory to define material properties and functions, hence the dependency on the modelled variables, as well as domain settings, boundary conditions and initial conditions.

3.2 Computer-Aided Design and Simulation

Computer-Aided Design (CAD) is the use of computer technologies that aid the design and documentation of a design (actions involved, modification, analysis and optimization). CAD software is used to pro-efficiently produce output files used for print, machining and other manufacturing processes.

Feature-based modelling allows a set of intrinsic geometric parameters to keep the original geometry relationship of the design following a certain regeneration. Setting dimensional constraints such as tangency, parallelism, and symmetry also fixes a cross-section geometry and favours parameterization. Through relations and equations, a fully parameterized model updates dimensions.

In the scope of specific physics analysis, refeaturing the model geometry with fillets and small patches ensures smooth surfaces and can solve missing connectivity information, erroneous shape information, tolerance issues, and more. Removing details like sliver faces in the scope of fluid dynamics can avoid anisotropic and high skewness (mesh elements with angular deviations from 90°) regions and denser meshes with bad element quality.

3.2.1 Mesh Refinement

The mesh generation process can be divided based on the topology of the elements that fill the domain. These two basic categories are known as structured and unstructured meshes.

An unstructured mesh is defined as a set of elements, commonly tetrahedrons, with defined connectivity. It is a more flexible choice for mesh generation. However, the solution accuracy may be relatively unfavourable compared to the structured mesh due to skewed elements in sensitive regions like boundary layers. A structured mesh is defined as a set of hexahedral elements with user-defined connectivity. It is a time-consuming task due to the possible need to break the domain manually into several blocks when the complexity of geometry increases.

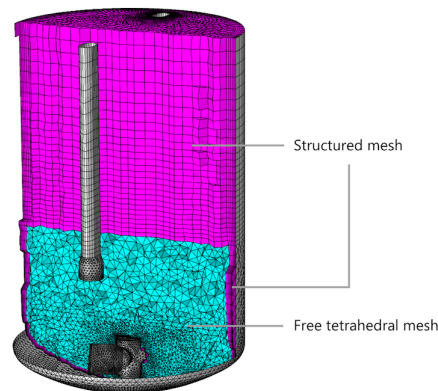


Figure 3.2: Structured and unstructured meshes [54]

Creating a refined mesh defines a finalized and discretized numerical model. A mesh convergence analysis estimates the accuracy of a simulation, meaning that the mesh should be finer defined in each spatial direction and the simulation carried out once again on the refined mesh. If the change in critical solution parameters for the original and finer mesh is within the required tolerance, the solution can be regarded as being mesh-converged. Another mesh quality parameter is the mesh growth rate, explained as the change in element size between neighbouring elements, a parameter to control the different surface transitions, and it should be small to achieve accuracy.

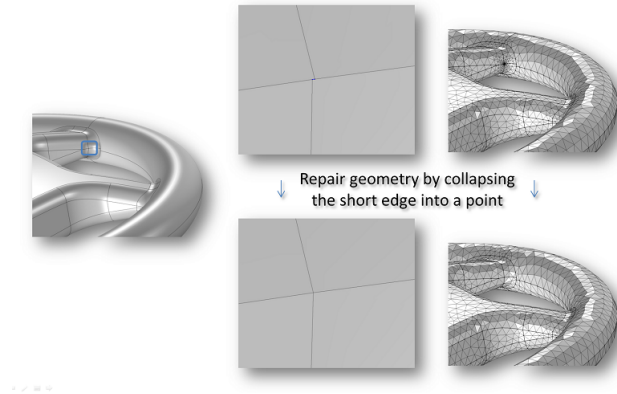


Figure 3.3: Defeaturing in mesh refinement [54]

3.2.2 Computational Fluid Dynamics

The mathematical representation of these systems (scaffold and bioreactor) can be achieved following **continuum** or **discrete** models.

With the continuum approach, an averaged description of the system behaviour based on the assumption that cells and tissue occupy the same space as continuous materials, the fluid dynamics theory can be used to infer interactions between material phases. Despite the drawback of lacking individual cell-scale data, continuum modelling provides sufficient information about the chemical and mechanical environment in constructs.

Discrete models treat the system as separate entities combined, using algorithms to determine cell fate, modelling individual cell movements, inter-cellular interaction and recreating signalling pathways. With a better understanding of the stochastic-level nature presented in tissue formation, discrete models aim to improve the fundamental understanding of cellular-level processes. However, the high computational cost linked to the non-existence of experimentally measured parameters of cellular behaviour make the discrete modelling impossible to account for large cell population and ill-suited for evaluating overall bioreactor systems.

3.2.3 Modelling the flow environment: Navier-Stokes Equations

Continuum models use the Navier-Stokes continuity equation for mass conservation (3.1) and a vector equation of momentum conservation (3.2) to describe the flow of free culture media.

$$\frac{\partial \rho}{\partial t} + \nabla \cdot (\rho \mathbf{u}) = 0 \quad (3.1)$$

$$\rho \left(\frac{\partial \mathbf{u}}{\partial t} + \mathbf{u} \cdot \nabla \mathbf{u} \right) = \rho g - \nabla p + \mu \nabla^2 \mathbf{u} \quad (3.2)$$

Where:

- ρ is the density (SI unit: kg/m^3)
- \mathbf{u} is the velocity vector (SI unit: m/s)
- p is the pressure (SI unit: Pa)
- ρg is the body force due to gravity
- μ is the dynamic viscosity (SI unit: $N \cdot s/m^2$)

The left side of equation (3.2) describes the inertial forces - the first term is time-dependent momentum change, and the second term is a convection momentum change - whereas the right side includes the pressure force, gravity force and viscous force. The equation is solved to obtain \mathbf{u} , the velocity field, and the pressure profile, to further assert the mechanical forces exerted on the scaffold.

As the media is considered to be an incompressible Newtonian fluid with constant viscosity and density, the incompressible flow formulation for small temperature variation with constant ρ flow takes the equation of motion reduced to:

$$\rho \nabla \cdot \mathbf{u} = 0 \quad (3.3)$$

All gases and many liquids are considered Newtonian fluids. The dynamic viscosity of a fluid, μ (*SI unit* : $Pa \cdot s$), is a measure of its resistance to deformation rate (viscosity = shear stress/rate of shear strain), and it is dependent on the thermodynamic state, not on the velocity field. Applications used during this project were isothermal flows since the Navier-Stokes equation for energy conservation was not considered. Also, incompressible fluids were considered. In that way, the coupling of equations of energy and the other equations is weak and can be considered entirely independently.[55]

3.2.3.1 Laminar and Turbulent Flow Regimes

The Reynolds number gives the ratio between inertial and viscous forces. Laminar flows have low Reynolds numbers, hence viscous forces dominate and tend to damp out all disturbances. High Reynolds numbers characterize turbulence, a chaotic flow field state in which the damping is very low, with disturbances growing by nonlinear interactions. Stokes flow behaviour is associated with small Reynolds numbers and is modelled with the Navier-Stokes equation, excluding the inertia term. This is called a creeping flow regime and is often appropriate for small channel and microfluidic applications. The laminar flow remains under a specific critical value of Reynolds number (for a pipe flow, the critical value is known to be approximately 2000). The dimensionless variable is defined by the following:

$$Re = \frac{\rho UD}{\mu} \quad (3.4)$$

Where ρ is the fluid density, U is the fluid velocity and D is the diameter of the pore (theoretically defined by a pipe).

3.2.3.2 Modelling the mechanical environment: Wall Shear Stress

Fluid flow magnitude can determine fluid shear stress exerted on the scaffold walls. The following equation can calculate the total shear stress:

$$WSS = \sqrt{\tau_{xy}^2 + \tau_{yz}^2 + \tau_{xz}^2} \quad (3.5)$$

Where,

$$\tau_{xy} = \mu \left[\frac{\partial u}{\partial y} + \frac{\partial v}{\partial x} \right], \tau_{yz} = \mu \left[\frac{\partial v}{\partial z} + \frac{\partial w}{\partial y} \right], \tau_{xz} = \mu \left[\frac{\partial u}{\partial z} + \frac{\partial w}{\partial x} \right] \quad (3.6)$$

, being u , v and w the three elements of velocity in the x , y and z directions, respectively, in the Cartesian coordinate system. As a tensor quantity requiring magnitude and orientation (given by first subscript - direction of the axis to which plane of action of shear stress is normal - and second subscript - direction of action of the shear stress), shear stress is positive when both the vector normal to the surface of action and the shear stress act in the same direction [56].

3.2.3.3 Modelling mass transport: Permeability

Mathematically, permeability can be represented as the proportionality constant between the fluid or gas velocity through the material, and the pressure gradient driving the flow. This relationship can be expressed using Darcy's law, which states that the volume flow rate of fluid through a porous material is proportional to the pressure difference across the material and inversely proportional to the fluid viscosity, meaning that the flux occurs in the direction of the pressure drop and is reduced as viscosity increases.

$$k = \frac{Q\mu L}{A\Delta P} \quad (3.7)$$

Where k is the permeability of the material expressed in m^2 , Q is the volume flow rate expressed in m^3/s , A is the cross-sectional area of flow expressed in m^2 , ΔP is the pressure difference across the material, L is the length of the flow path, and μ is the fluid viscosity expressed in $Pa.s$. Darcy's law can only be applied to laminar flow with constant viscosity, being necessary to assert about the Reynolds Number of the flow. Previous studies [57] and [58] explained the effectiveness of applying Darcy's law for $Re \leq 1$, with Re values up to 8.6 giving an insignificant variation. For analysing flow that present a Reynolds number higher than 8.6, it's preferred than Forchheimer equation or Ergun equation, both of which take into consideration the presence of inertial forces.

3.2.3.4 Wall Boundary Conditions

Slip Condition

The Slip option prescribes a no-penetration condition, $u \cdot n = 0$. From a modelling point of view, this can be a reasonable approximation if the wall's main effect is preventing fluid from leaving the domain. It is implicitly assumed that there are no viscous effects at the slip wall; hence, no boundary layer develops.

No Slip Condition

No slip is the default boundary condition for solid model walls. A no-slip wall is a wall where the fluid velocity relative to the wall velocity is zero. For a stationary wall, that means that $u = 0$. As a result, the heat transfer from the solid surface to the fluid layer adjacent to the surface is by pure conduction since the fluid is motionless. Assuming a no-slip condition at the wall, the motionless layer slows down the particles at the neighbouring fluid layers due to friction of adjacent layers.

Considering the flow of a fluid over a flat plate, the velocity of the fluid is uniform, at U_∞ , approaching the plate. Thus, the fluid can be considered adjacent layers on top of each other. The plate is felt up to some distance, beyond which the fluid velocity remains unchanged. This region is called the velocity boundary layer, meaning that the viscous effects and the velocity changes are significant.

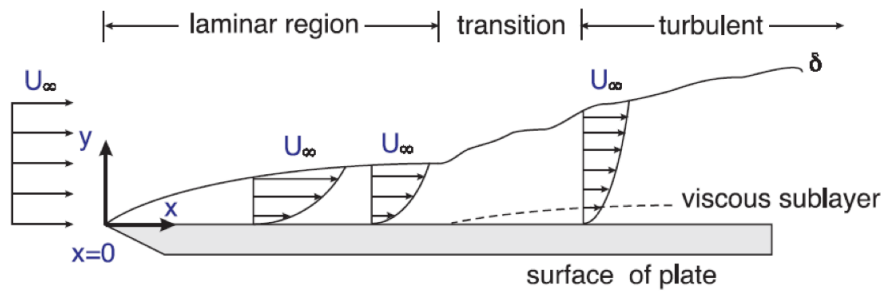


Figure 3.4: Wall Boundary schematics. adapted from [4]

Boundary layer effects are considered when a high Reynolds number (turbulent flows) reflects the fluid friction environment. Regarding the example given of flow past a flat plate with a local Reynolds number based on a fixed distance from a leading edge ($x=0$), experimental data indicate that for $Re < 2 \times 10^5$, the boundary layer is laminar, for $2 \times 10^5 < Re < 3 \times 10^6$ the boundary layer may be either laminar or turbulent and for $3 \times 10^6 < Re$ the boundary layer is turbulent. [56]

3.2.3.5 Solvers

The nonlinear solver method depends if the model solves a stationary or time-dependent problem.

A fully coupled, damped Newton method is applied in the stationary case for finding the iterative solution for the differentiable function. The initial damping factor is low since a full Newton step can be harmful unless the initial values are close to the final solution. The nonlinear solver algorithm automatically regulates the damping factor to reach a converged solution.

In the time-dependent case, the initial guess for each time step is the previous time step, which is a very good initial value for the nonlinear solver. The automatic damping algorithm is then not necessary. The Newton method's damping factor is set to a constant value slightly smaller than one.

Numerically ill-conditioned models can arise as a consequence of extreme variations in the material properties, or high aspect ratio geometry, meaning that the

system matrix is nearly singular and that it will be difficult to solve on a finite-precision computer.

Computational Methods

4.1 Computer Aided Design of Scaffolds

SolidWorks[®] (Dassault Systèmes SolidWorks Corp., Waltham, MA, USA) was the modelling software for creating the 3D models of scaffolds. Based on previous studies [59], four rectangular-shaped scaffold configurations with different angular lay-down patterns ($0\text{-}30^\circ$, $0\text{-}45^\circ$, $0\text{-}60^\circ$ and $0\text{-}90^\circ$) were designed, with size, shape and distribution of void channels (pores) regular and interconnected. Dimensions considered were $(10.75 \times 7.45 \times 3.05)mm$, with $250 \mu m$ in filament diameter distanced by a pore size of $550 \mu m$, layered 10 times and interconnected by a 10% of each strut thickness to increase structural integrity (parameters presented in Table 4.1). Moreover, a pore size gradient was added to four constructs, with sizes of 1.12, 0.85, 0.70, 0.66, 0.58, 0.55 and $0.52 \mu m$ symmetrically distributed along the lay-down layer (see Figure 4.2).

This approach aims to mimic the variations in microarchitecture, namely the porosity in the cortical bone, and the trabecular structure of cancellous bone. *Rothweiler, R. et al* [52] have conducted a comparison study between alveolar and iliac bone, and have found values in cortical and trabecular porosity. Cortical porosity, comprising vascular porosity with its intracortical pore system (IPS), presented values from 5% to 24%.

For mass transport within scaffolds, one hypothesis of this work relies on knowing whether a gradient or constant porosity determine a well distributed range of wall shear stress values and assert on the overall permeability changes. According to literature, the gradient pore distribution can enhance cell penetration at the high porosity zones at the scaffold/tissue interface, while improving mechanical load-bearing with low porosity zones [60].

The scaffold porosity was calculated following the equation:

$$\varphi_{Design} = \left(1 - \frac{V_{CAD}}{V_{Bulk}}\right) \times 100 \quad (4.1)$$

Where, V_{CAD} is the occupied volume and V_{Bulk} is the bulk volume of the CAD model. For this work, eight different geometries were considered, with different levels of porosity for each of them, either constant or graded distributed. These models will be henceforth be referred to by their angular orientation value and modality of porosity, for example a 0-30° patterned scaffold with constant porosity will be called 30NORM.

A feature-based parametric solid model consists of two key elements: a feature tree, and fully parameterized sketches employed for protruding solid features. a fully parameterized sketch implies that the sketch profile is fully constrained and dimensioned, so that a change in dimension value yields a rebuilt in accordance with design intents (as seen in Figure 4.1). The parameters were adapted so that the scaffold would have a total dimension similar to the works of *Bartolo et al* [12] and could match a critical size for bone defects applications. A note should be made about the parameter "Number of Filaments along y-axis". The actual number of fibers only matches the defined value when layers are rotated 90° apart. When the angle between layer is different, the scaffold will have a different number of fibers in that layer, however the size along the x-axis remains the same.

Global Variable	Description	Value (mm)
Scaffold_Length	Length of scaffold	10.750
Pore_Size	Determines pore size	0.550
Filament_Diameter	Determines fiber width	0.250
Filament_Intersection	Determines height difference between rotated layers (tangential contact area)	0.050
Filament_Number_along_y-axis	Number of filaments along a layer	10
Filament_Number_along_x-axis	Number of filaments along a layer	10
Number_of_repetitions_of_layers	Number of filaments along a layer	10

Table 4.1: Parameters used for CAD Design of Scaffolds

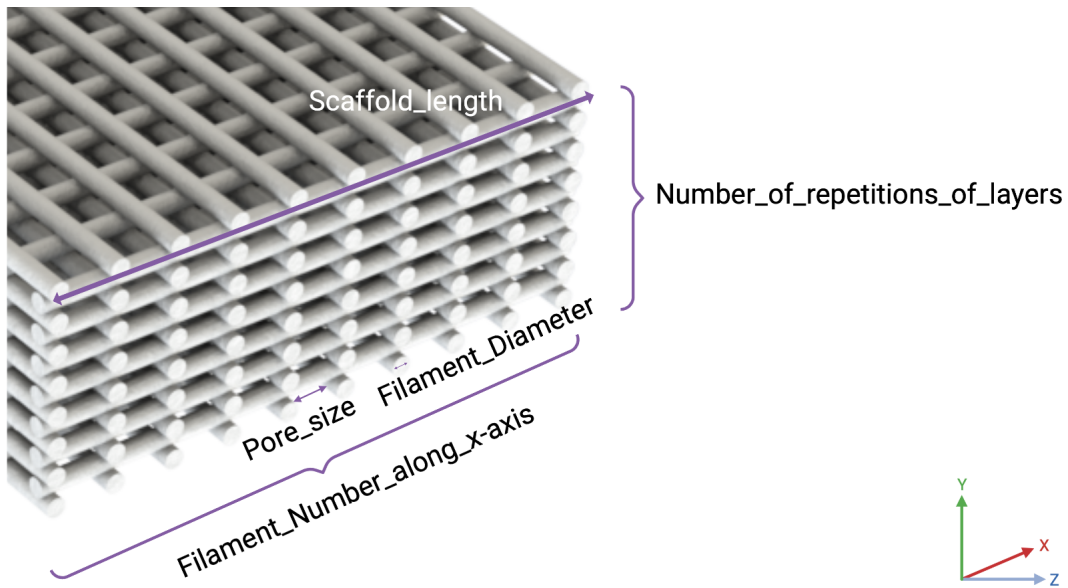


Figure 4.1: Parameters used for CAD Design of Scaffolds

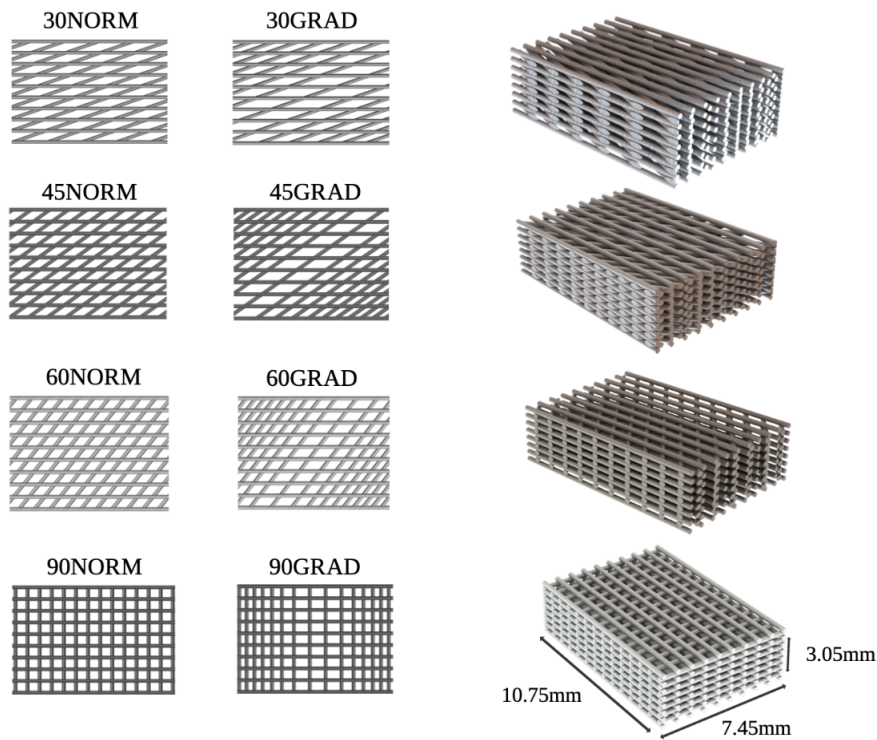


Figure 4.2: Computer-Aided Designs of Scaffolds

An important parameter for scaffold characterization and predicted performance is porosity. Taking advantage of software tools to measure the fiber and total volume of the construct, approximated values for total porosity were calculated. The fiber cross-sectional area of contact between adjacent layers was considered to be a

4. Computational Methods

square shape, as an approximation of the shape of the filament extruded by Fused Deposition Modelling (FDM). It would be possible to assert on the fidelity of the 3D-Printing if experimental porosity data was available, since extrusion manufacturing could affect fiber width and create pore occlusions.

	0-30°	0-45°	0-60°	0-90°
Pores of 550 μm	69%	60%	63%	68%
Pores of 1120, 850, 700, 660, 580, 555, 552 and 550 μm	68%	67%	68%	67%

Table 4.2: Average of porosity in the models considered

4.2 Computational Fluid Dynamics

Computational Fluid Dynamics provides insights into complex *in vivo* processes, comprising also the physiology, biology and biochemistry within the biological extent of this particular study. Micro-scale of cell culture and blood vessels, and its translation into biological fluid simulation, is challenging and expensive in terms of computational cost (translating one behavior at one scale to a resulting one at another scale). For example, at a microscopic scale, the fluid molecule size becomes comparable to the domain size, as the continuum assumption of fluid, formulated in the Navier-Stokes equations (listed in Chapter 3) can no longer be applied, and molecular dynamics have to describe molecular motion regimes. Using Finite Element Method, incorporating this microscale becomes limitative.

Finite element method analysis was performed using the CFD module from COMSOL Multiphysics software (version 5.2a, www.comsol.com, Stockholm, Sweden). The Laminar Flow (*spf*) physics interface was selected, considering a stationary study, to find which input fluid velocity values originate optimal numerical flow stimulation conditions according with the experimental studies of *Bartolo et al.* in [59] [61]. It is frequently prohibitive to model large scaffold volumes, so often the preferred option reduces the model to a representative smaller geometry, being helpful to diminish the high-demanding computational cost as well for further quantification of macro-scale errors and reliability evaluation [3].

4.2.1 Model Geometry

Taking in account the periodicity of all geometries, the reduced representation models consists in a rectangular shaped chamber that encapsulates the construct, with extended vertical void segments of 1.15 *mm* in both sides. In order to investigate the influence of scaffold architecture on flow stimulus, a representative Volume of Interest (VOI) of 1/4 of the designed models was the case-of-study geometry used during simulations, as seen in figure 4.3.

4.2.2 Applied Boundaries and Assumptions. Fluid Domain.

In a perfusion bioreactor, the inlet fluid enters the scaffolds homogeneously from the top surface of the 3D-printed scaffolds, to a bottom outlet. For that matter, a series of boundary conditions and assumptions were considered.

The fluid was modeled as a fully developed incompressible Newtonian fluid,

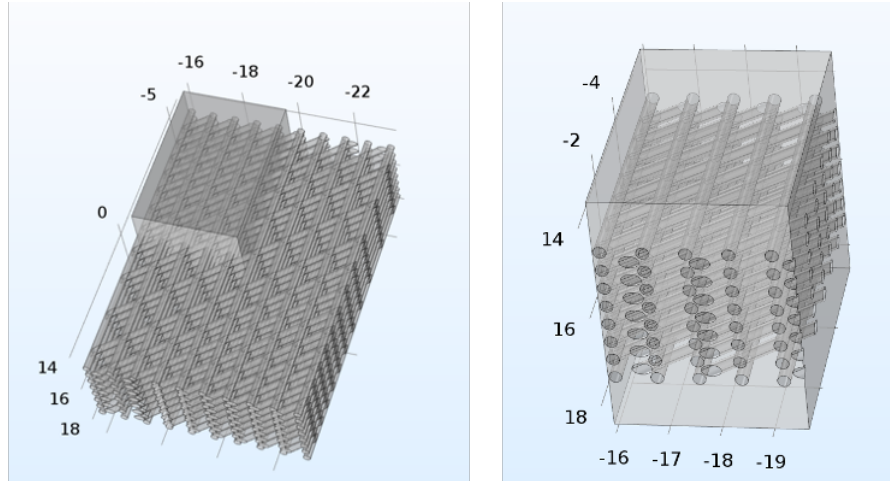


Figure 4.3: Model Geometry setup - VOI and Scaffold - for COMSOL Multiphysics software (version 5.2a, www.comsol.com, Stockholm, Sweden)

based on culture medium with a density of 1000 Kg/m^3 and a viscosity of $0.0037 \text{ Pa}\cdot\text{s}$, similar to a cell culture media with 5% wt/wt Dextran, based on previous documentation [59]. Moreover, Deqiang *et al.* [62] have experimentally supplemented media with different percentages of dextran, a tackifier, and shown that, with a constant flow rate, a positive proportionality happens with viscosity, through increasing dextran supplementation, and flow shear stress. The magnitude of the inlet flow rate (0.1, 0.25, 0.50, 0.75 and 1 mm/s) was chosen based on that in peristaltic pumps (range 0.02 to 1 mL/min) generally used in experimental and simulation studies on perfusion bioreactors [63] [64].

- The average fluid pressure at the outlet surface of the scaffolds is set to zero (Gauge Pressure);
- A stationary linear problem was formulated, since it is time-invariant. Time-dependent studies should be used in high-Reynolds number regime as these flows tend to become inherently unsteady. In this case, The fluid flow was considered laminar since the fluid velocity was low ($< 1200 \mu\text{m/s}$) in combination with micro-dimension of channel width inside scaffolds, mimicking small diameters of blood vessels and arterioles ($Re \ll 2000$);
- Large arteries blood flow exert high values of shear rate, allowing blood to be treated as a Newtonian fluid. [65]. For this study, the fluid behaves as a Newtonian fluid, as it is assumed to have a constant viscosity, independently of velocity gradients;
- Fluid does not slip at the wall, implying that the fluid in contact with the wall

is stationary. Therefore, the walls of the perfusion chamber were modelled as closed walls with no slip condition;

- The surface of the constructs was assumed to be smooth, although its noted that roughness can change the fluid interaction with the scaffold structures [66], and solid, being that the physical-chemical composition of the constructs could be undefined;
- The equations solved by the Laminar Flow (*spf*) interface are the Navier-Stokes equations for conservation of momentum and the continuity equation for conservation of mass.

4.2.3 Mesh Convergence Study

One of the considerable aspects of FEM analysis is the dependency of its result accuracy on the mesh size, since a model with coarse mesh is not representative of the continuous model and leads to deviation from exact results. Mesh convergence analysis is important in FEA as it helps to determine the minimum mesh density required to accurately capture the physical behavior of the system being modeled.

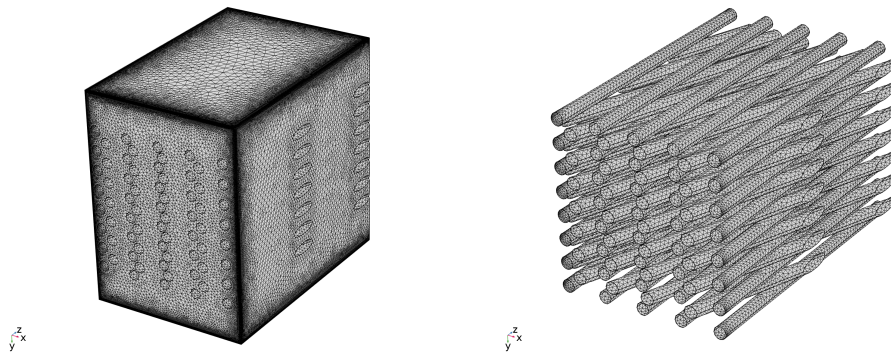


Figure 4.4: Mesh display for the conducted simulation of 30GRAD

Mesh convergence analysis involves progressively refining the mesh to see how it affects the solution. A well-converged mesh will produce consistent results with further refinement, indicating that the solution has stabilized and can be trusted. Performing a mesh convergence analysis helps to avoid over- or under-meshing, which can lead to unreliable or inaccurate results.

Thus, a mesh sensitivity analysis was performed with constantly increasing the number of elements to reach mesh size-independent results. After performing this analysis on the studied geometries, a suitable mesh size on the FEM models was obtained for analysis. The average wall shear stress of the fluid domain was the

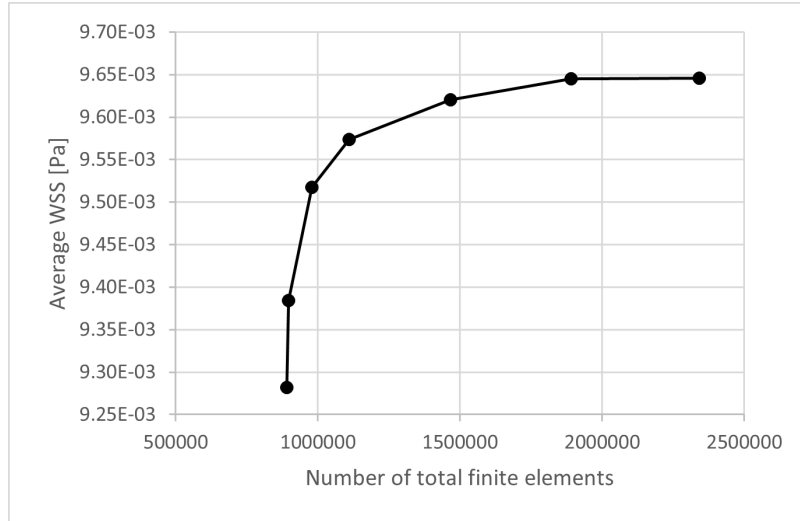


Figure 4.5: Mesh Convergence Study for the average Wall Shear Stress value

variable in which a mesh independence study was conducted, as shown in Figure 4.5 and described in 4.3, to assure that results are numerically independent of the mesh size for whole patterns.

	30NORM	30GRAD	45NORM	45GRAD	60NORM	60GRAD	90NORM	90GRAD
Number of Elements	1891537	2021290	1867873	1916750	2100408	1894773	1948868	2088801
Average Element Quality	0.681	0.683	0.681	0.680	0.680	0.678	0.683	0.682
Average Growth Rate	1.976	1.973	1.975	1.975	1.979	1.975	1.973	1.976

Table 4.3: Mesh features and quality parameters.

Different meshes were built with increased fixed elements through the 8 edges of the perfusion setup. The maximum difference in the calculated average fluid velocity and fluid shear stress between the sixth mesh, with normal element size and 300/310/310 elements in x/y/z directions, respectively, and the seventh, with fine element size, was 5%, which was considered negligible. Therefore, the finite element meshes with normal element sizes listed in the table 4.3 were assumed to be fine enough to accurately determine the fluid velocity and wall shear stress distribution inside the 3D-scaffold in the perfusion setup. The computation time used for mesh generation was between 3-5 minutes, the average element quality was 0.681, termed as a good value for FEA applied to CFD, and the average growth rate was 1.975.

Results and Discussion

5.1 Influence of different inter-filament orientation and porosity on velocity magnitude

Fluid simulations of *Laminar Flow (spf)* were conducted for the VOI in each model geometry of scaffolds. The fluid enters at a flow velocity of 0.1 mm/s from an inlet on top to the bottom surface, and since no slip boundary condition was assumed, the gradient of fluid velocity enhanced near the filament surfaces.

The essayed perfusion chamber provided a strong forward flow, without having any flow recirculation zones, within the scaffolds, increasing to 0.6 mm/s in 30NORM, 0.8 mm/s in the 30GRAD, 0.6 mm/s in 45NORM to 0.7 mm/s in 45GRAD, 0.5 mm/s in 60NORM, 0.7 mm/s in 60GRAD, 0.5 mm/s in 90NORM and 0.7 mm/s in 90GRAD, which suggests that the presence of a graded distribution of pore sizes as well as filament orientation had not a relative effect on the velocity magnitude but a considerable effect in its distribution.

We can predict on the level of WSS distributed uniformly from the plots given. With increased velocity variation, less uniform will be the distribution of fluid-induced stresses along the construct. The regions of maximum acceleration were the pore gaps between strands, as the minimum were the peripheral regions and wall planes. Since the fluid has the tendency to flow in the medium between the strands and there was an effect of the pressure difference between inlet flow and outlet flow in the VOI, the exit fluid velocity was higher than the entrance fluid velocity.

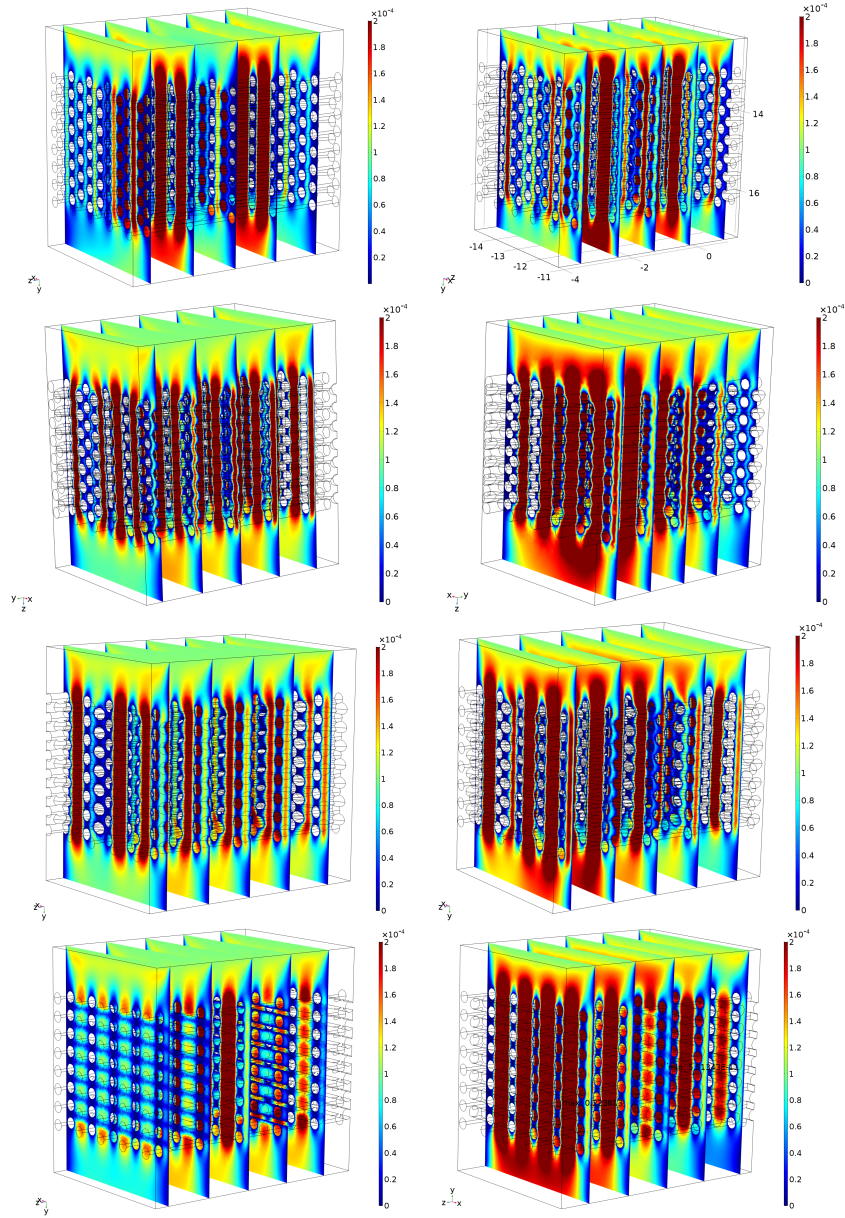


Figure 5.1: Simulations of the velocity magnitude distribution are presented on 2D plot groups using COMSOL Multiphysics. The left side of the plot displays the 30NORM, 45NORM, 60NORM, and 90NORM geometries from top to bottom. On the right side, the 30GRAD, 45GRAD, 60GRAD, and 90GRAD geometries are shown from top to bottom.

5.2 Influence of different inter-filament orientation, porosity and flow velocity on Wall Shear Stress

This section presents CFD simulation results regarding wall-shear stress inside the scaffolds. Understanding the distribution of wall shear stress on the scaffolds allows to identify heterogeneity within the constructs surface. Previous documentation had shown that a non-uniform cell differentiation is caused by heterogeneous WSS distribution. Results for an inlet flow velocity of 0.1 mm/s are shown in the following page.

In accordance with [67], the fluid shear stress magnitude and distribution coincided with the fluid velocity gradient, thus showing maximum values in the pore gaps region, and minimum in the outer region of the scaffolds. Overall, the distribution and magnitude of WSS increased by decreasing angular orientation of filaments (as seen in figure 5.2).

Fluid induced shear stress values presented in previous documentation reports ranges from $1 \times 10^{-4} Pa$ to $1.2 Pa$ for human cell lines induction of osteogenic and angiogenic lineages, and ranges 0.8 to 3.0 Pa as a result of interstitial fluid movement through *lacunae*, caused by deformation and tension under loading [34]. A statistics study of distribution curves and modality of this variable, upon an area wall percentage for inlet flows of 0.1 mm/s, 0.25 mm/s, 0.50 mm/s, 0.75 mm/s and 1 mm/s, was conducted in the eight different geometries.

The values for WSS with increments of inlet velocities showed a linear increase in average, maximum and minimum WSS, for all geometries. At 1 mm/s, the perfusion flow rate produced high shear stresses ($> 30 mPa$), and the maximum shear stress value of 370 mPa occurred for the 45NORM model. As reported through studies [68], low perfusion rates increase osteoblast proliferation while high rates ($> 1 ml/min$) are associated with cell death. In every distribution, approximately 50% of the scaffolds, under a perfusion flow velocity of 1 mm/s, were compromised with high WSS values, associated with cell wash-out and apoptosis [47] [48], stating evidences on the perfusion rate influence upon scaffold culturing. At an inlet flow velocity of 0.25 mm/s, 30NORM and 60NORM showed lower percentage of WSS values above 30 mPa, opposing to its graded configurations. As for the 0-45° oriented scaffolds, 45GRAD showed less values above 30 mPa than 45NORM, and for the 0-90° oriented scaffolds, no significant changes occurred.

5. Results and Discussion

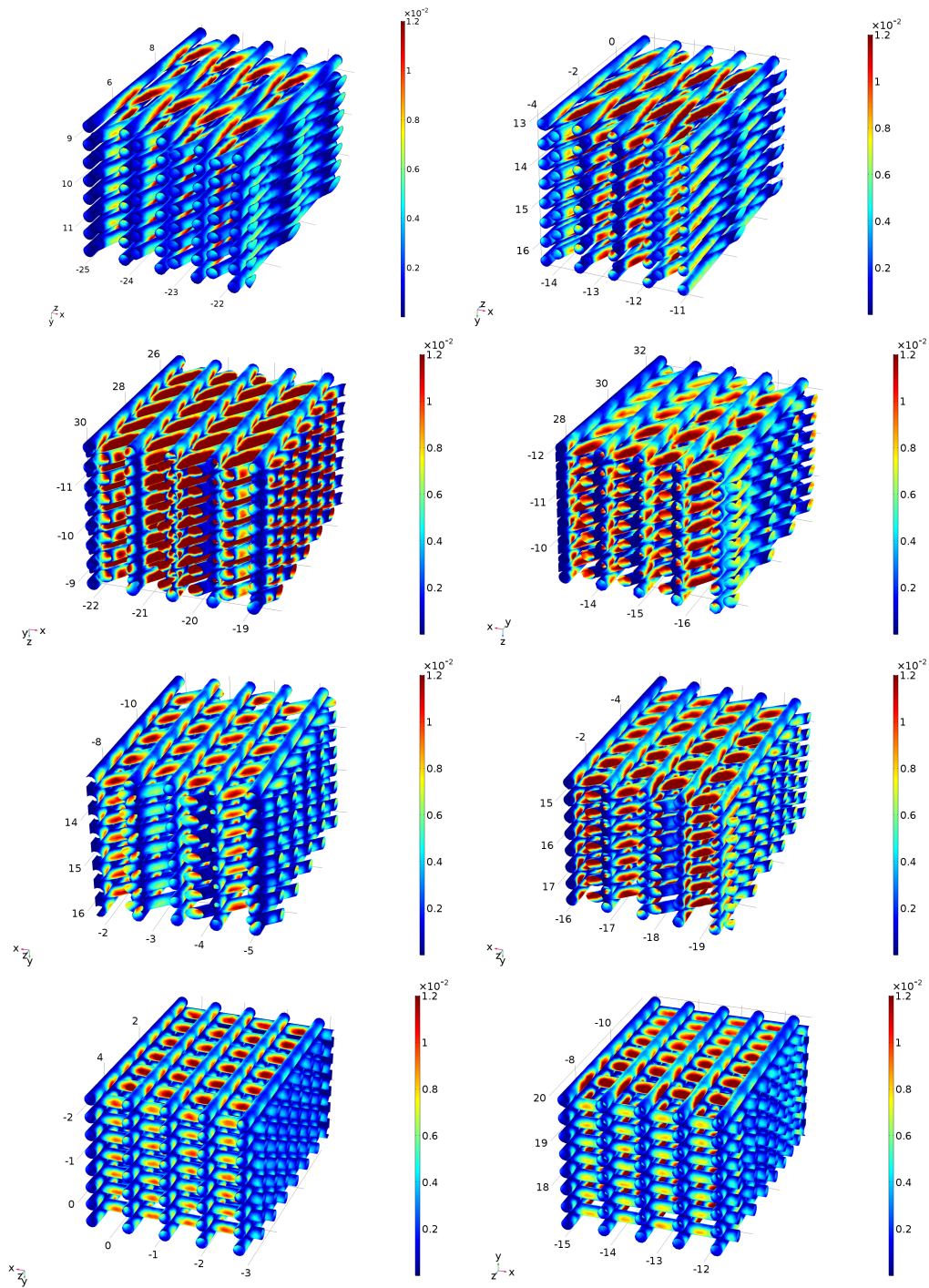


Figure 5.2: Simulations of the WSS distribution are presented on 3D plot groups using COMSOL Multiphysics. The left side of the plot displays the 30NORM, 45NORM, 60NORM, and 90NORM geometries from top to bottom. On the right side, the 30GRAD, 45GRAD, 60GRAD, and 90GRAD geometries are shown from top to bottom.

5. Results and Discussion

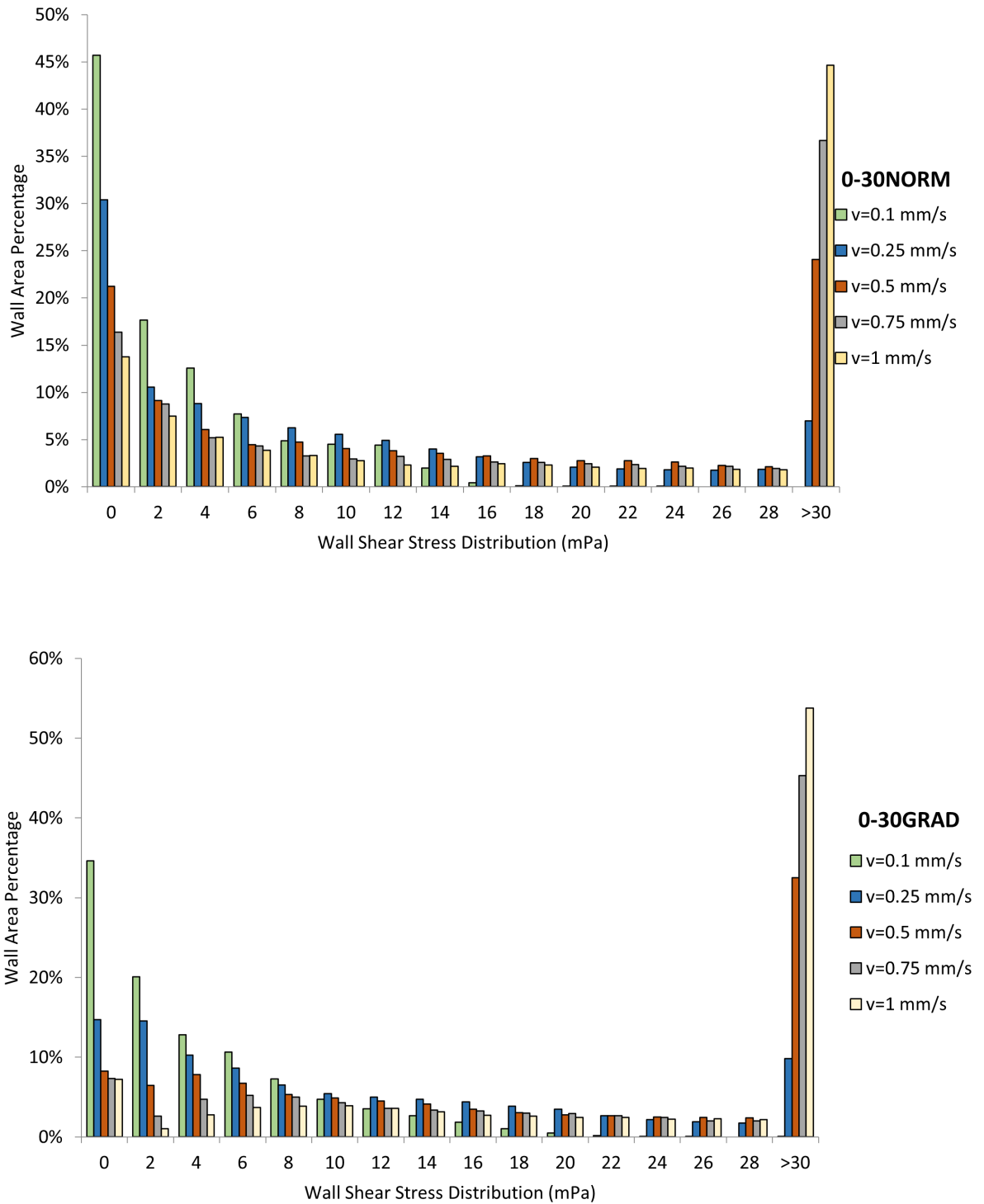


Figure 5.3: WSS Distribution over wall area, expressed as percentage, for 0-30° angular oriented scaffolds

5. Results and Discussion

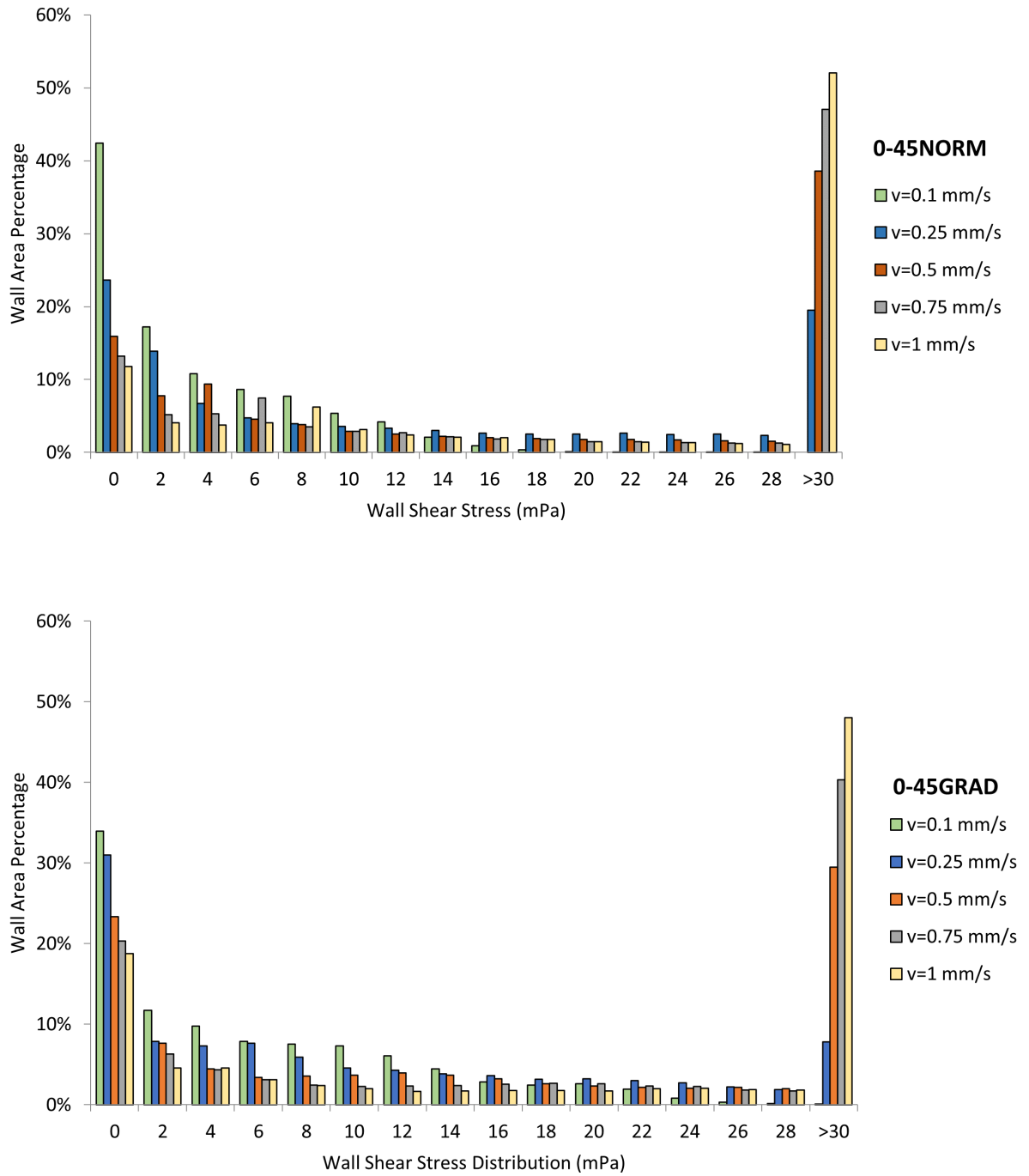


Figure 5.4: WSS Distribution over wall area, expressed as percentage, for 0-45° angular oriented scaffolds

5. Results and Discussion

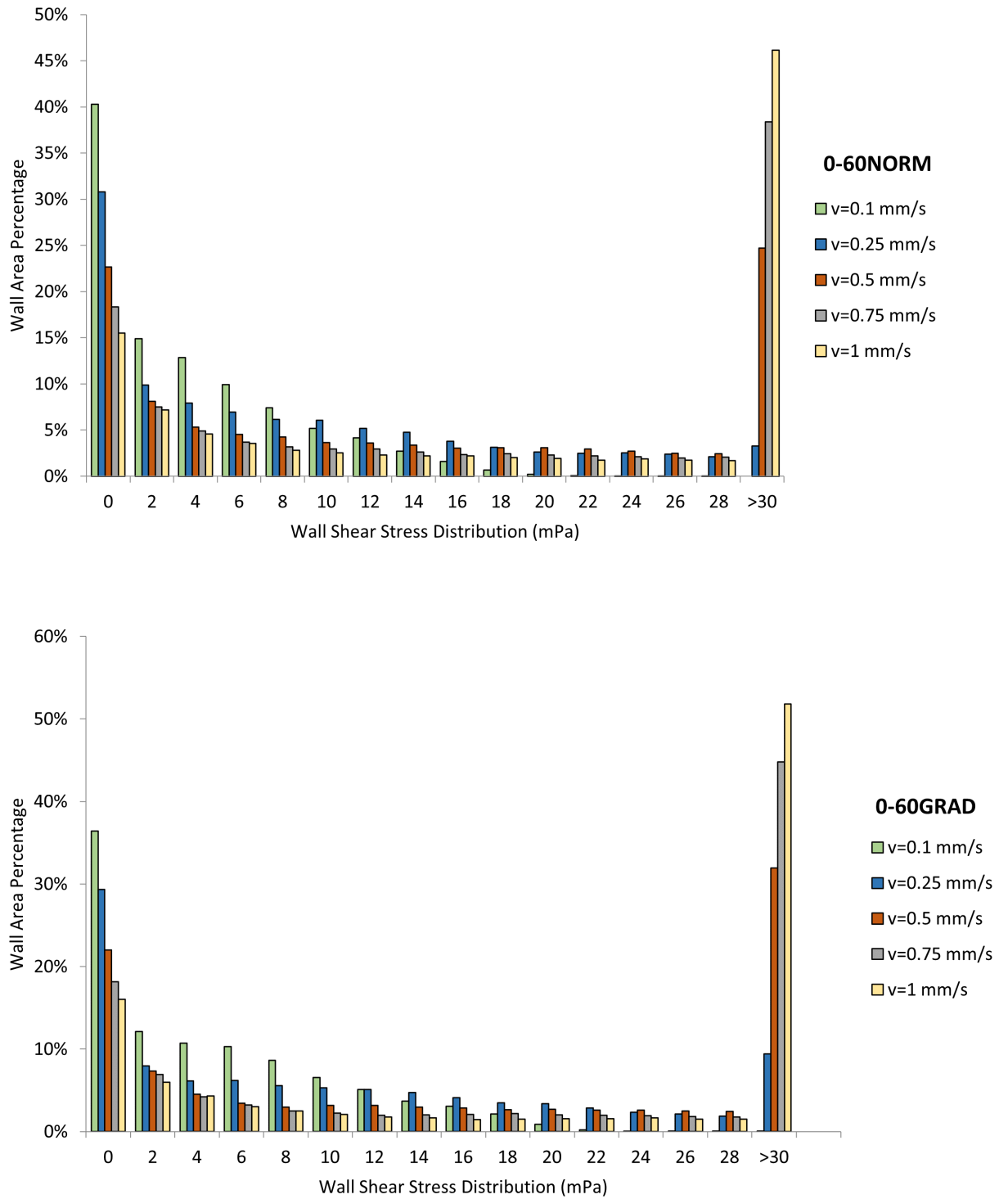


Figure 5.5: WSS Distribution over wall area, expressed as percentage, for 0-60° angular oriented scaffolds

5. Results and Discussion

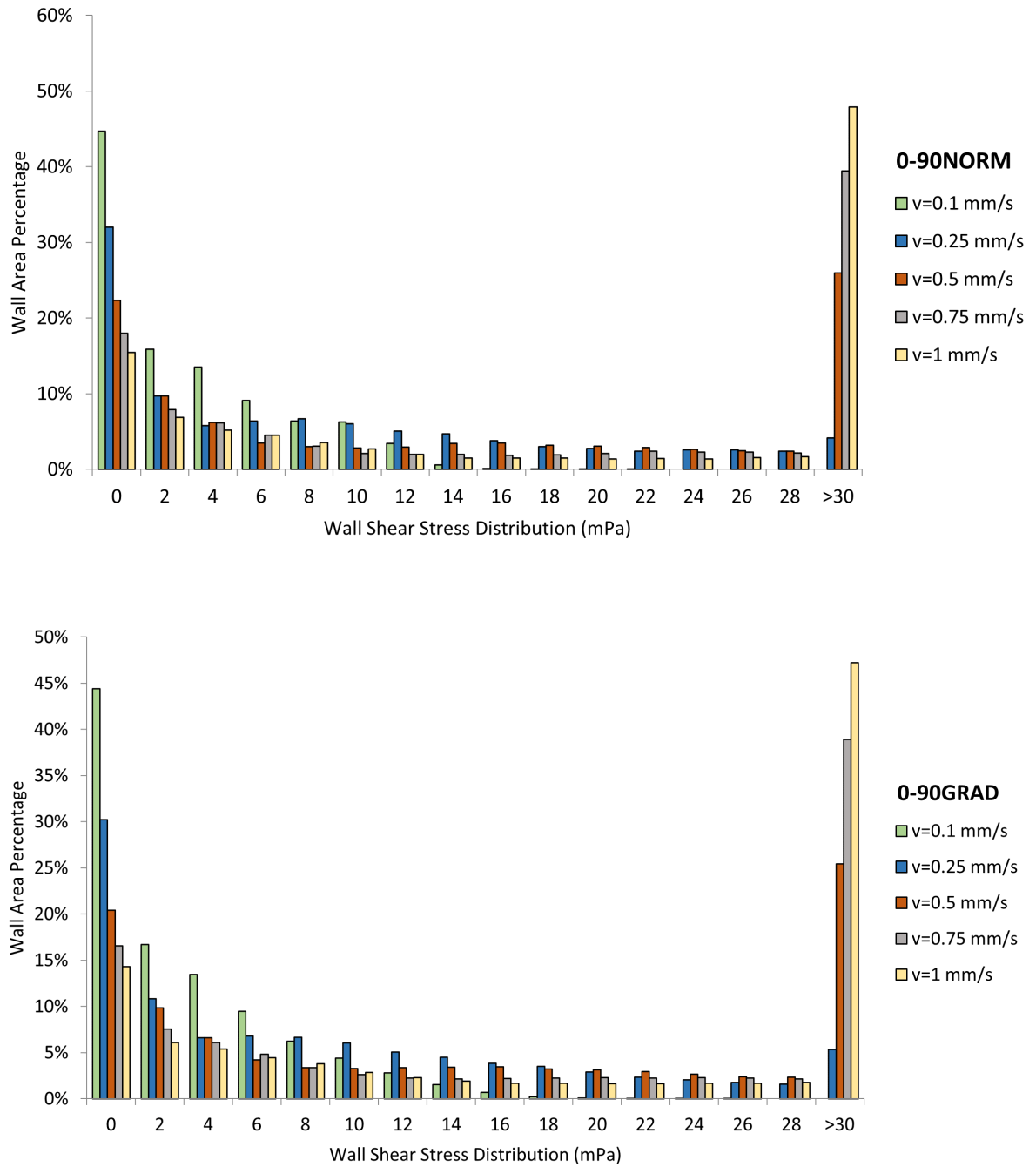


Figure 5.6: WSS Distribution over wall area, expressed as percentage, for 0-90° angular oriented scaffolds

5. Results and Discussion

Hence the WSS values under low flow rates favored the range values reported in Table 2.2 for osteogenic stimulation, differentiation and proliferation, a statistics analysis of inlet flows with velocities of 0.1 *mm/s* and 0.25 *mm/s* revealed more accurate results to assert on the distribution.

Inlet flow velocity of 0.1 mm/s.

	30NORM	30GRAD	45NORM	45 GRAD	60NORM	60GRAD	90NORM	90GRAD
MEDIAN	3.86	3.39	4.85	2.79	2.55	3.25	2.75	2.68
MEAN	2.43	4.96	6.84	4.27	3.72	4.62	3.84	3.89
SD	4.10	4.67	6.68	4.45	3.70	4.68	3.85	4.02
SKEW	1.22	1.28	0.97	1.10	0.98	1.08	0.95	1.22
KURT	0.68	1.24	0.14	0.54	0.03	0.52	-0.09	1.06
CV	1.69	0.94	0.98	1.04	1.00	1.01	1.00	1.03

Table 5.1: Statistical analysis for an inlet flow velocity of 0.1 mm/s.

Inlet flow velocity of 0.25 mm/s.

	30NORM	30GRAD	45NORM	45GRAD	60NORM	60GRAD	90NORM	90GRAD
MEDIAN	6.07	8.49	8.48	6.97	6.37	8.12	6.86	6.69
MEAN	9.66	12.4	15.88	10.67	9.29	11.54	9.6	9.74
SD	10.24	11.67	18.03	11.12	9.25	11.69	9.63	10.05
SKEW	1.22	1.28	1.48	1.1	0.98	1.08	0.95	1.22
KURT	0.68	1.24	2.07	0.54	0.03	0.52	-0.01	1.06
CV	1.06	0.94	1.14	1.04	1.00	1.01	1.00	1.03

Table 5.2: Statistical analysis for an inlet flow velocity of 0.25 mm/s.

Non-equally distributed WSS is given by a larger than zero coefficient of variance (CV). As the distribution curves show us, all geometries had similarly a non-uniform distribution, with an improved exception for the 30GRAD, and the model 30NORM for the less-uniform distribution. As for the skewness value (SKEW), models of 60NORM and 90NORM showed the lowest values. Even though presenting values higher than zero, meaning that values of WSS greater or smaller than the mean (MEAN) values were distributed asymmetrically in each distribution tails, those were the stand-out models. Kuortosis (KURT) measures tail-heaviness of distributions (range of variation of WSS), and the heaviest and lightest tails measured were 30GRAD and 90NORM, respectively. Over-viewing the results given, 30GRAD model showed the best performance regarding WSS distribution upon its surface walls.

Also, for optimal regulation of WSS, allowing cell proliferation and/or differentiation, 60NORM provides the best choice due to low dispersion of values, given by the standard deviation (SD), compared to other angular orientations, in both inlet

velocities. In contrast, 45NORM presented a more dispersed distribution of WSS, suggesting that a small change in the bioreactor's flow rate will affect more the in-between strand surface of the construct (in accordance to [67]). Overall, for both inlet velocities, the mean values and standard deviation values favored the 60NORM and 90NORM geometries, but 60NORM summed up all the statistics topics for the best choice of scaffold configuration. As for the 30NORM geometry, even though its mean value was the lowest at 0.1 mm/s , the standard deviation value was the highest, meaning that the cells were not subjected to the same stimulus of wall shear stress, and this low uniformity crossed off this geometry.

5.3 Influence of different scaffold micro architecture on Permeability

The knowledge of the arrangement of the pore network is not only important for mineralization kinetics and mechanotransduction but also for the dynamics of the transport of biologics involved in graft regeneration [69] [70]. Concerning the studied geometries, with a regular arrangement of pores, the structural parameter of tortuosity (previously explained in Chapter 2) is linked to the scaffold permeability, being that it is expected that a low tortuosity ratio value conducts to a more permeable construct, and as this value increases, the less-permeable is the construct.

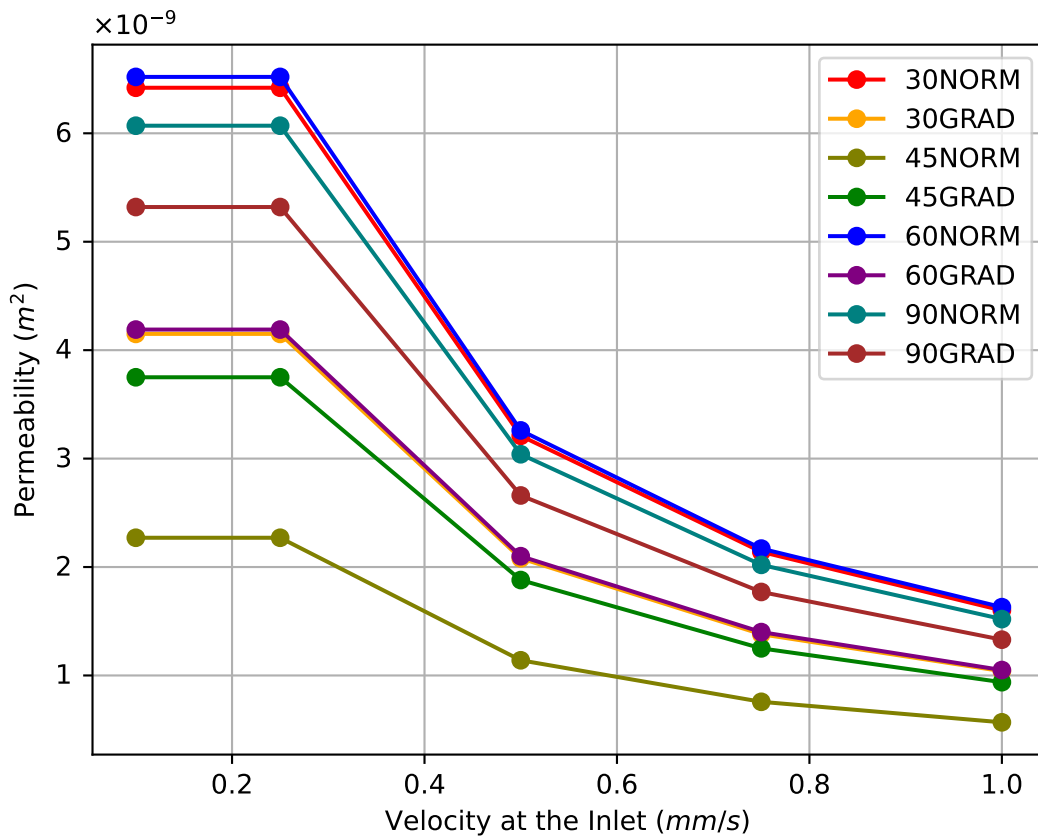


Figure 5.7: Permeability values with inlet flow velocities of 0.1 mm/s, 0.25 mm/s, 0.5 mm/s, 0.75 mm/s and 1 mm/s, for all configuration geometries of scaffolds

At an inlet velocity of 0.1 mm/s and 0.25 mm/s, the highest permeability values were observed for the 30NORM and 60NORM geometries, while the lowest permeability values were observed for the 45NORM and 45GRAD geometries. As the inlet velocity increased to 0.5 mm/s, the highest permeability values were again

observed for the 30NORM and 60NORM geometries, but the 90GRAD geometry also showed relatively high permeability values. The lowest permeability values were still observed for the 45NORM and 45GRAD geometries. At an inlet velocity of 0.75 mm/s and 1mm/s, the permeability values continued to decrease for all scaffold geometries, with the 30NORM and 60NORM geometries still showing the highest values and the 45NORM and 45GRAD geometries still showing the lowest values.

Overall, it appears that the permeability of the scaffolds is influenced by both the geometry of the scaffold and the inlet velocity of the fluid flowing through it. Biological efficiency of the scaffold, in terms of pore architecture, relies on a higher permeability, as it conducts to bone tissue formation (while low permeability leads to cartilaginous tissue formation).

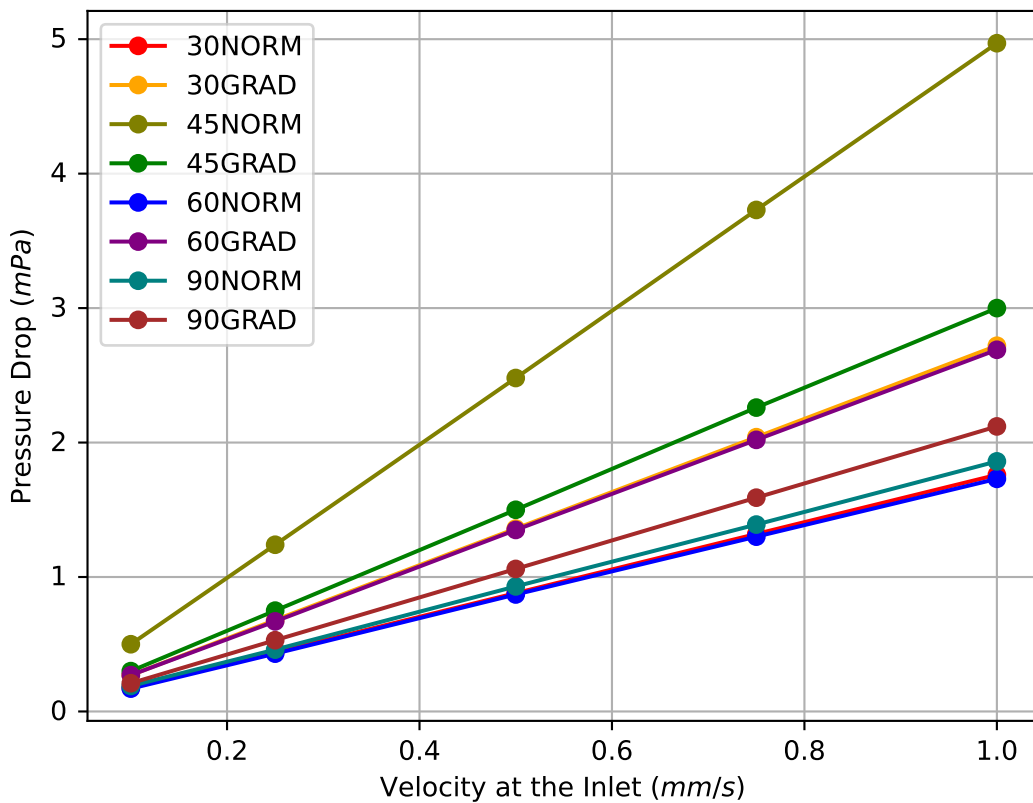


Figure 5.8: Pressure variation values with inlet flow velocities of 0.1 mm/s, 0.25 mm/s, 0.5 mm/s, 0.75 mm/s and 1 mm/s, for all configuration geometries of scaffolds

According to ranged values, higher inlet velocities decrease the permeability of the construct. The 30NORM and 60NORM geometries consistently showed the

highest permeability values across all inlet velocities tested, while the 45NORM and 45GRAD geometries consistently showed the lowest values. Comparing the values from Table 2.3, 45NORM is the best choice as it presents the lowest permeability values.

The variation of pressure, as data for permeability calculus, was also verified through the average value of pressure in the top and bottom layers of the construct (figure 5.8). The non-stochastic arrangement of pores allows us to assert on how does the level of tortuosity affects the pressure variation. As the angle deviation decreases, the pressure variation increases.

Overall, for the Wall Shear Stress and permeability values, as factor for a suitable iliac bone scaffold, suggested that 30GRAD and 60GRAD were the best geometries.

Conclusions

Along this work, evidences on the stimulus of fluid shear stress for bone cell behavior have been assessed in regards to computational modelling tools. Overall, the wall shear stress values pointed out the 30GRAD and 60NORM configurations, and permeability values suggested that 30GRAD and 60GRAD were the best geometries, meaning that the graded porosity helped positively for a well-suitable iliac bone scaffold.

Initially, a grid independence study was undertaken, showing that for a certain grid refinement yielding, the accuracy showed a mild increase, and therefore, results converged for values with low relative differences.

The perfusion bioreactor setup was the optimized system for studying how scaffold geometry and inlet velocity affects fluid-induced parameters, concluding that, in accordance to previous studies, the ranges for differentiation and proliferation were confirmed.

Hopefully, this work can bridge the gap between bone tissue engineering research on modelling setups and the translation into clinically available bone tissue engineering applications.

Future Work

The present models lack experimental validation of the estimated shear stress distribution, since quantifying fluid dynamics would only be possible using laser Doppler velocimetry or particle image velocimetry, affecting cell growth inside the construct.

Furthermore, equating hydrostatic compression or substrate deformation onto the mechanical environment, as an extension of this work, is needed. Adding to the mechanical behavior study, there is the need for accounting time-dependent phenomena, such as culture after seeding, because as the cells fill up the spaces within the pores and surround themselves with ECM, the obstruction of the pores result in different values of WSS, due to decreased porosity and shielding effect of ECM. Considering the possibility of seeding cells in these scaffolds and of placing the cell-seeded constructs within bioreactors, it is essential to avoid detrimental effects caused by high shear stresses or insufficient nutrient and waste transfer.

Regarding permeability, Darcy's law revealed flaws in its ineffectiveness in situations in which the fluid is non-Newtonian fluid. Ali and Sen [71] concluded, after comparing the application of Darcy's law for both a Newtonian based model for blood and a non-Newtonian counterpart, that the non-Newtonian flow of blood caused almost twice the magnitude of WSS originating from Newtonian blood flow, due to differences in their viscosity behaviors. This means that although the law is perfectly suitable for more basic analyses, special consideration must be given not only to the Reynolds number of the fluid flow as well as the viscosity properties of the studied fluid.. Although this simplification takes place, blood can behave as a non-Newtonian fluid for lower shear rates in small vessels, once the viscosity increases with decreasing shear rate (shear-thinning fluid)

Finally, another important point to be studied is the oxygen supply for cell culture. A low oxygen concentration could be a limiting effect on cell culture. The biological fluid contains dioxygen that flows inside the porous material. Therefore,

7. Future Work

fluid mechanics equations at the macroscale must be coupled with diffusion equations and oxygen consumption equations to ensure a whole distribution of nutrients inside the porous media, because the process of perfusion into a scaffold takes too much time during the *in vitro* experiment, the manipulations are complex and the process takes time and is expensive. *Digital twins* can effectively create an accurate computational representation of the scaffold physics.

Bibliography

- [1] W. Xiao, Y. Wang, S. Pacios, S. Li, and D. T. Graves, “Cellular and Molecular Aspects of Bone Remodeling. ,” 9-16, *Frontiers of Oral Biology* (, 2016.
- [2] A. Gleadall, D. Visscher, J. Yang, D. Thomas, and J. Segal, “Review of additive manufactured tissue engineering scaffolds: relationship between geometry and performance. ,” 1-16, *Burn. Trauma* 6, 2018.
- [3] I. Burova, I. Wall, and R. Shipley J, “Mathematical and computational models for bone tissue engineering in bioreactor systems,” *Journal of Tissue Engineering*, vol. 10:1-25, 2018.
- [4] M. Bahrami, “Forced Convection Heat Transfer ,” *ENSC 388 Engineering Thermodynamics and Heat Transfer*, 2011.
- [5] G. Turnbull and et al., “3D bioactive composite scaffolds for bone tissue engineering,” *Bioact. Mater.* 3, 2018.
- [6] C. Mandrycky, K. Phong, and Y. Zheng, “Tissue engineering toward organ-specific regeneration and disease modeling,” *MRS Commun*, 2017.
- [7] A. R. Amini, C. T. Laurencin, and S. P. Nukavarapu, “Bone Tissue Engineering: Recent Advances and Challenges,” *Crit Rev Biomed Eng.*, 2012.
- [8] N. Cubo-Mateo and L. Rodríguez-Lorenzo, “Design of Thermoplastic 3D-Printed Scaffolds for Bone Tissue Engineering: Influence of Parameters of “Hidden” Importance in the Physical Properties of Scaffolds,” *Polymers*, 2020.
- [9] H. Seddiqi, A. Saatchi, G. Amoabediny, M. N. Helder, S. A. Ravasjni, M. S. H. Aghaei, J. Jin, B. Zandieh-Doulabi, and J. Klein-Nulen, “Inlet flow rate of perfusion bioreactors affects fluid flow dynamics, but not oxygen concentration in 3D-printed scaffolds for bone tissue engineering: Computational analysis and experimental validation,” *Computers in Biology and Medicine*, 2020.

- [10] J. Möller and R. Pörtner, “Digital Twins for Tissue Culture Techniques—Concepts, Expectations, and State of the Art,” *Processes* 9, 447, 2021.
- [11] L. Geris, T. Lambrechts, A. Carlier, and I. Papantoniou, “The future is digital: In silico tissue engineering,” *Curr. Opin. Biomed. Eng.* 6, 92–98, 2018.
- [12] A. M. Abdalla M. Omar, M. H. Hassan, E. Daskalakis, G. Ates, C. J. Bright, Z. Xu, E. J. Powell, W. Mirihanage, and P. Bartolo, “Geometry-Based Computational Fluid Dynamic Model for Predicting the Biological Behavior of Bone Tissue Engineering Scaffolds,” *Journal of Functional Biomaterials*, 2022.
- [13] R. Florencio-Silva, G. R. Silva Sasso, E. Sasso-Cerri, M. J. Simões, and P. S. Paulo Sérgio Cerri, “Biology of Bone Tissue: Structure, Function, and Factors That Influence Bone Cells,” *Biomed Res Int.*, 2015.
- [14] T. Ghassemi, A. Shahroodi, M. H. Ebrahimzadeh, A. Mousavian, J. Movaffagh, and A. Moradi, “Current Concepts in Scaffolding for Bone Tissue Engineering ,” *Arch Bone Jt Surg.* 6(2): 90–99., 2018.
- [15] W. L. Grayson, D. Marolt, S. Bhumiratana, M. Fröhlich, X. E. Guo, and G. Vunjak-Novakovic, “Optimizing the medium perfusion rate in bone tissue engineering bioreactors ,” 1159-1170, *Biotechnology and bioengineering*, 2011.
- [16] M. Bohner, Y. Loosli, and L. D. Baroud G., “Commentary: Deciphering the link between architecture and biological response of a bone graft substitute,” *Acta Biomaterialia*, 2011.
- [17] S. Weiner and H. Wagner, “The Material bone:Structure-Mechanical Function Relations,” *Annu. Rev. Mater. Sci.*, 1998.
- [18] X. Tong, I. S. Burton, J. S. Jurvelin, H. Isaksson, and H. Kröger, “Iliac crest histomorphometry and skeletal heterogeneity in men,” *Bone Reports* 6, *Elsevier Inc.*, 2017.
- [19] F. L. Bach-Gansmo, A. Brüel, M. V. Jensen, E. N. Ebbesen, H. Birkedal, and J. S. Thomsen, “Osteocyte lacunar properties and cortical microstructure in human iliac crest as a function of age and sex,” *Elsevier Inc.*, 2016.
- [20] “Coloured scanning electron micrograph (sem) of cancellous (spongy) bone.” Available at <https://www.mediastorehouse.co.uk/science-photo-library/bone-tissue-6447959.html>.

- [21] “Lm of compact bone, showing a haversian system.” Available at <https://www.sciencephoto.com/media/301625/view/lm-of-compact-bone-showing-a-haversian-system->.
- [22] V. Sikavitsas, J. Temenoff, and A. Mikos, “Biomaterials and bone mechanotransduction ,” *2581-2593, Biomaterials*, 2001.
- [23] P. Schmitz, C. C. Neumann, C. Neumann, M. Nerlich, and S. Dendorfer, “Biomechanical analysis of iliac crest loading following cortico-cancellous bone harvesting,” *Journak of Orthopaedic Surgery and Research*, 2018.
- [24] S. A. Zijderve, C. M. ten Bruggenkate, J. P. A. van Den Bergh, and E. A. J. M. Schulten, “Fractures of the iliac crest after split-thickness bone grafting for preprosthetic surgery: report of 3 cases and review of the literature.,” *J Oral Maxillofac Surg*, 2004.
- [25] J. Henkel, M. Woodruff, D. Epari, and et al., “Bone Regeneration Based on Tissue Engineering Conceptions — A 21st Century Perspective ,” *216-248, Bone Res 1*, 2013.
- [26] N. Ansari and N. A. Sims, “The Cells of Bone and Their Interactions,” *Springer, Cham*, vol. 262, 2020.
- [27] S. Vedi, Kaptoge, and J. Compston, “Age-related changes in iliac crest cortical width and porosity: a histomorphometric study,” *Journal of Anatomy*, 2011.
- [28] C. Murphy, F. J. O’Brien, D. G. Little, and A. Schindeler, “Cell-scaffold interactions in the bone tissue engineering triad ,” *Eur Cell Mater*, 2013.
- [29] A. Gaharwar, I. Singh, and A. Khademhosseini, “Engineered biomaterials for in situ tissue regeneration,” *Nat. Rev. Mater.*, 2020.
- [30] A. Gaharwar, I. Singh, and A. Khademhosseini, “Conventional and Recent Trends of Scaffolds Fabrication: A Superior Mode for Tissue Engineering,” *Pharmaceutics*, 2022.
- [31] S. Arabnejad, R. Johnston, J. Pura, B. Singh, M. Tanzer, and D. Pasini, “High-strength porous biomaterials for bone replacement: a strategy to assess the interplay between cell morphology, mechanical properties, bone ingrowth and manufacturing constraints,” *Acta Biomater.*, 2016.
- [32] A. Cheng and et al., “Advances in Porous Scaffold Design for Bone and Cartilage Tissue Engineering and Regeneration ,” *14-29, Tissue Eng. - Part B Rev. 25*, 2019.

- [33] S. Sundelacruz and D. L. Kaplan, "Stem cell- and scaffold-based tissue engineering approaches to osteochondral regenerative medicine ," 464-655, *Semin. Cell Dev. Biol.* 20, 2009.
- [34] R. J. McCoy and F. J. O'Brien, "Influence of Shear Stress in Perfusion Bioreactor Cultures for the Development of Three-Dimensional Bone Tissue Constructs: A Review," *TISSUE ENGINEERING: Part B*, 2010.
- [35] A. Wubneh, E. Tsekoura, C. Ayranci, and H. Uludag, "Current State of Fabrication Technologies and Materials for Bone Tissue Engineering," *Acta Biomaterialia*, 2018.
- [36] S. Bose, S. Vahabzadeh, and A. Bandyopadhyay, "Bone tissue engineering using 3D printing ," *Volume 16, Issue 12. Materials Today*, 2013.
- [37] "Finite element mesh refinement." Available at <http://home.att.net/castleisland>.
- [38] J. Harvestine, T. Gonzalez-Fernandez, A. Sebastian, and et al., " Osteogenic preconditioning in perfusion bioreactors improves vascularization and bone formation by human bone marrow aspirates ," *Sci Adv*, 2020.
- [39] A. Pasini, J. Lovecchio, G. Ferreti, and E. Giordano, "Medium Perfusion Flow Improves Osteogenic Commitment of Human Stromal Cells," *Stem Cells International*, vol. 2019, 2018.
- [40] N. Pearson, J. Oliver, R. Shipley, and et al., "A multiphase model for chemically- and mechanically- induced cell differentiation in a hollow fibre membrane bioreactor: minimising growth factor consumption," *Biomech Model Mechanobiol*, 2016.
- [41] Y. Guyot, B. Smeets, T. Odenthal, and et al., "Immersed boundary models for quantifying flow-induced mechanical stimuli on stem cells seeded on 3D scaffolds in perfusion bioreactors," *PLoS Comput Biol*, 2016.
- [42] L. Freed, J. Marquis, R. Langer, and et al., "Kinetics of chondrocyte growth in cell-polymer implants," *Biotechnol Bioeng*, 1994.
- [43] V. Sikavitsas, G. Bancroft, J. Dolder, T. Sheffield, J. Jansen, C. Ambrose, and A. Mikos, "Fluid flow increases mineralized matrix deposition in 3d perfusion culture of marrow stromal osteoblasts in a dose dependent manner," *Proc Natl Acad Sci USA*, vol. 1, 01 2002.

- [44] A. S. Goldstein, T. M. Juarez, C. D. Helmke, M. C. Gustin, and A. G. Mikos, “Effect of convection on osteoblastic cell growth and function in biodegradable polymer foam scaffolds,” *Biomaterials*, 2001.
- [45] S. Yamada, M. Yassin, T. Schwarz, J. Hansmann, and K. Mustafa, “ Induction of osteogenic differentiation of bone marrow stromal cells on 3D polyester-based scaffolds solely by subphysiological fluidic stimulation in a laminar flow bioreactor ,” *Journal of Tissue Engineering*, 2021.
- [46] M. Raimondi, F. Boschetti, L. Falcone, G. Fiore, A. Remuzzi, E. Marinoni, M. Marazzi, and R. Pietrabissa, “ Mechanobiology of engineered cartilage cultured under a quantified fluid-dynamic environment. ,” *69-82, Biomechanics and Modeling in Mechanobiology 1*, 2002.
- [47] S. Cartmell, B. Porter, A. Garcia, and R. Guldberg, “ Effects of medium perfusion rate on cell-seeded three-dimensional bone constructs in vitro. ,” *1197–1203, Tissue Engineering 9*, 2003.
- [48] M. Raimondi, M. Moretti, M. Cioffi, C. Giordano, F. Boschetti, K. Lagana, and R. Pietrabissa, “ The effect of hydrodynamic shear on 3D engineered chondrocyte systems subject to direct perfusion. ,” *215–222, Biorheology*, 2006.
- [49] F. Maes, T. Claessens, M. Moesen, V. Oosterwyck, P. Van Ransbeeck, and P. Verdonck, “ Computational models for wall shear stress estimation in scaffolds: A comparative study of two complete geometries ,” *1586-1592, Journal of Biomechanics*, 2012.
- [50] M. Grimm and J. Williams, “Measurements of permeability in human calcaneal trabecular bone ,” *743-745, Journal of Biomechanics 30 (7)*,, 1997.
- [51] E. Nauman, K. Fong, and T. Keaveny, “Dependence of intertrabecular permeability on flow direction and anatomic site ,” *517-524, Annals of Biomedical Engineering*, 1999.
- [52] R. Rothweiler, C. Gross, E. Bortel, S. Früh, J. Gerber, E. Boller, J. Wüster, A. Andres Stricker, T. Fretwurst, G. Iglhaut, S. Nahles, R. Schmelzeisen, B. Hesse, and K. Nelson, “Comparison of the 3D-Microstructure Between Alveolar and Iliac Bone for Enhanced Bioinspired Bone Graft Substitutes ,” *Frontiers in Bioengineering and Biotechnology*, 2022.
- [53] V. I. Sikavitsas, J. S. Temenoff, and A. G. Mikos, “Biomaterials and bone mechanotransduction ,” *2581-2593, Biomaterials*, 2001.

- [54] “Finite element mesh refinement.” Available at <https://www.comsol.com/multiphysics/mesh-refinement?parent=physics-pdes-numerical-042-32>.
- [55] O. Zienkiewicz, R. Taylor, and J. Zhu, “The Finite Element Method: Its Basis and Fundamentals,” *Elsevier, Oxford*, 2013.
- [56] J. Welty, G. Rorrer, and D. Foster, “Fundamentals of Momentum, Heat and Mass Transfer,” *Wiley*, 2014.
- [57] M. Chor and W. Li, “A permeability measurement system for tissue engineering scaffolds. Measurement Science and Technology, ,” *Biotechnol. Bioeng.*, 2006.
- [58] I. Ochoa, J. Sanz-Herrera, J. García-Aznar, M. Doblaré, D. Yunos, and A. Boccaccini, “Permeability evaluation of 45S5 Bioglass®-based scaffolds for bone tissue engineering ,” *Journal of Biomechanics*, 2009.
- [59] A. Fallah, M. Altunbek, P. Bartolo, G. Cooper, A. Weightman, G. Blunn, and B. Koc, “3D printed scaffold design for bone defects with improved mechanical and biological properties,” *Journal of the Mechanical Behavior of Biomedical Materials*, 2022.
- [60] F. Liu, Q. Ran, M. Zhao, T. Zhang, D. Zhang, and Z. Su, “Additively manufactured continuous cell-size gradient porous scaffolds: Pore characteristics, mechanical properties and biological responses in vitro,” *Materials*, vol. 13, p. 2589, 2020.
- [61] M. Domingos, F. Chiellini, A. Gloria, P. Ambrosio, P. Bartolo, and E. Chiellini, “Effect of process parameters on the morphological and mechanical properties of 3-D Bioextruded poly(ϵ -caprolactone) scaffolds,” *Rapid Prototyp.J.*, 2012.
- [62] L. Deqiang, T. Tingting, L. Jianxi, and D. Kerong, “Effects of Flow Shear Stress and Mass Transport on the Construction of a Large-Scale Tissue-Engineered Bone in a Perfusion Bioreactor,” *TISSUE ENGINEERING: Part A*, 2009.
- [63] S. Cartmell, B. Porter, A. García, and R. Guldborg, “Effects of Medium Perfusion Rate on Cell-Seeded Three-dimensional Bone Constructs in Vitro ,” *Tissue Eng.*, 2003.
- [64] R. McCoy, C. Jungreuthmayer, and F. O’Brien, “Influence of Flow Rate and Scaffold Pore Size on Cell Behavior During Mechanical Stimulation in a Flow Perfusion Bioreactor ,” *Biotechnol. Bioeng.*, 2012.

- [65] J. O'Connor, P. Day, P. Mandal, and A. Revell, "Computational fluid dynamics in the microcirculation and microfluidics," *Integrative Biology*, 2016.
- [66] D. Ali and S. Sen, "Computational Fluid Dynamics Study of the Effects of Surface Roughness on Permeability and Fluid Flow-Induced Wall Shear Stress in Scaffolds," *Ann. Biomed. Eng.*, 2018.
- [67] A. R. Saatchi, H. Seddiqi, G. Amoabediny, M. N. Helder, and B. Zandieh Doulabi, "Computational Fluid Dynamics in 3D-Printed Scaffolds with Different Strand-Orientation in Perfusion Bioreactors," *Iran J. Chem. Chem. Eng.*, 2020.
- [68] H. Seddiqi, A. Saatchi, G. Amoabediny, M. N. Helder, S. A. Ravasjani, M. Safari Hajat Aghaei, J. Jin, B. Zandieh-Doulabi, and J. Klein-Nulend, "Inlet flow rate of perfusion bioreactors affects fluid flow dynamics, but not oxygen concentration in 3D-printed scaffolds for bone tissue engineering: Computational analysis and experimental validation ," *Computers in Biology and Medicine*, 2020.
- [69] M. Marenzana and T. R. Arnett, " The Key Role of the Blood Supply to Bone ," *203-215, Bone research*, 2013.
- [70] S. Elsharkawy and A. Mata, "Hierarchical Biomineralization: from Nature's Designs to Synthetic Materials for Regenerative Medicine and Dentistry ," *Advanced healthcare materials*, 2018.
- [71] D. Ali and S. Sen, "Permeability and fluid flow-induced wall shear stress of bone tissue scaffolds: Computational fluid dynamic analysis using Newtonian and non-Newtonian blood flow models ," *201-208, Computers in biology and medicine*, 2018.